University of Alberta

Thin Film pH Measuring Device

by

Jia luo

A thesis submitted to the Faculty of Graduate Studies and Research
in partial fulfillment of the requirements for the degree of

Master of Science

in

Materials Engineering

Department of Chemical and Materials Engineering

Fall 2011
Edmonton, Alberta

Abstract

This thesis presents research on the selection and development of thin film deposition of materials and initial data on the integration of a pH measuring device suitable for evaluation. This device used two particular tantalum compounds deposited by dc magnetron reactive sputtering as functional layers. Key parameters to film quality, such as resistivity, optical constants, composition, and pH response will be discussed in detail. Results indicated that nitrogen gas flow both controls the resistivity of sputtered tantalum nitride and suppressed the incorporation of oxygen. Variable Angle Spectroscopic Ellipsometer transmission scan on tantalum oxide with various oxygen pressure indicated insulating oxide forms only when the target enters oxide mode at 10^{+} sccm of oxygen flow. X-ray Photo-electron Spectroscopy surveys on tantalum oxide films showed that stoichiometric tantalum pentoxide was deposited. Preliminary result on pH response of the devices indicated the resistance increased with increasing pH.

Acknowledgement

I am deeply grateful to my supervisor, Dr Kenneth Cadien, for his outstanding support and supervision during my graduate program. This thesis would not be possible without his incredible patience, exceptional guidance, and constant support.

I also would like to thank Les Schowalter and Scott Munro, who had trained me on the tools of the Nanofab. Special thanks to Leslie Cadien for her generous help in reviewing the manuscript.

I sincerely thank Ali Foroughi, Lucy Nolan, Can Xu, and others in our research group for their help and encouragement.

Finally, I would like to honor my parents, who had given me so much of their love and support during my whole life.

Table of Content

List of Figures

List of Tables

Conversion for pressure from Torr to Pa:

1 Torr = 133.322 Pa

Chapter 1: Introduction

1.1. Objective of Research

This research was part of a project to build a thin film pH measuring device. Such a device has many applications in medical, agricultural, and industrial environments by reducing the footprint and cost for pH monitors. For example, normal blood pH is between 7.35 and 7.45, but when human bodies go into shock their blood pH drops to the lower end of the range. Current pH measurements immerse a conventional pH electrode in a blood sample. A disposable pH measuring chip inserted in hand held readers would reduce the volume of blood required and would allow users such as athletes and emergency workers to inspect blood pH on site.

The goal of this project is (a) to design the masks, (b) select the materials for the resistors, ion conducting dielectric, and the electrodes, (c) develop the deposition process for these materials, (d) integrate the fabrication processes and the masking layers, and (e) perform an initial characterization of the finished device. Figure 1.1 shows a photograph of a finished device and the cross-sectional view of its internal structures with color showing the materials used in each layer.

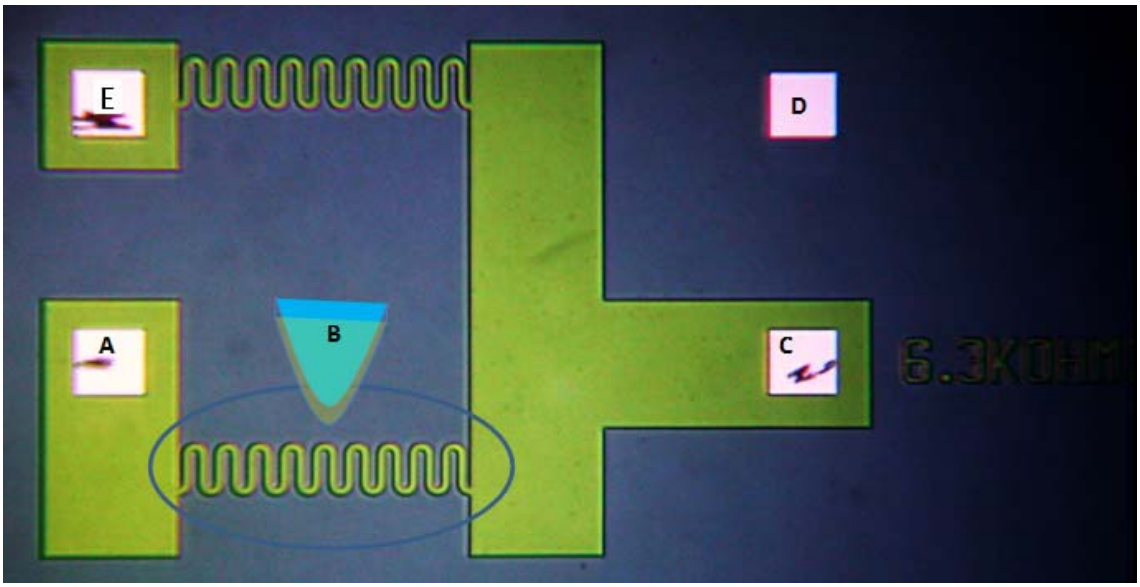

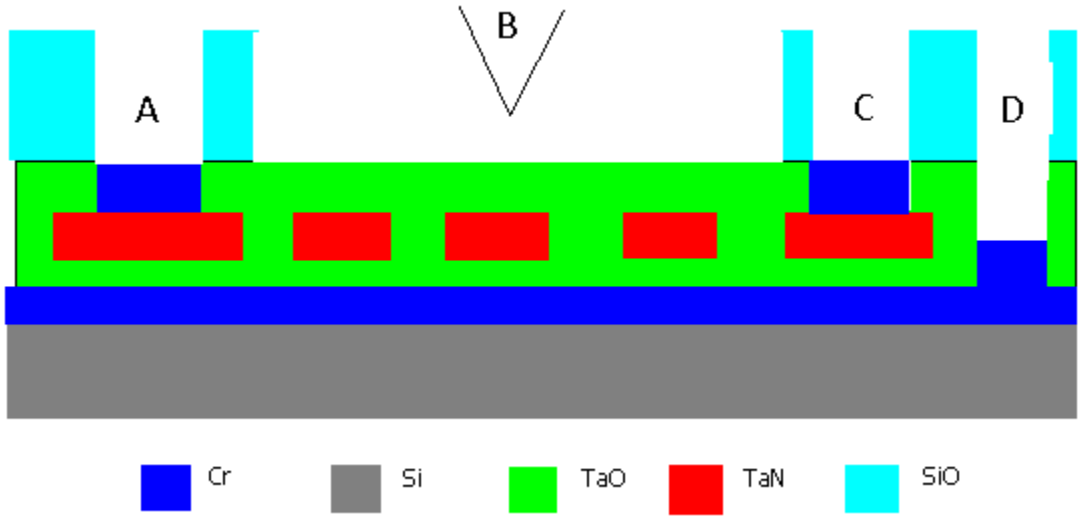

Figure 1.1: The design and materials used to fabricate a thin film pH measuring device

1.2. Organization of Thesis

This thesis starts with a literature review of tantalum, tantalum nitrides, and tantalum oxides and is followed by the history and working principles of common

pH measurement techniques, ion sensitive field effect transistors (ISFET), and ion conductors. Then the chapter ends with the principles of sputtering, reactive sputtering, and dc magnetron sputtering.

Chapter 3 introduces and explains the experimental methods and procedures for depositing and fabricating the sample films and devices along with the description of each tool used in the processes. Explanations for design decisions for the device and process parameters and characterization methods will be included in this section.

Results and discussions are detailed in chapter 4. Resistivity of the TaN films, optical properties of the Ta_2O_5 films, and their composition with respect to reactive gas flow will be given and discussed. There will be some preliminary results from finished devices, and their significance are discussed.. The problems that appeared during this project will be discussed along with how they affect the design of the device. The conclusion and future plans for development are in the last chapter.

Chapter 2: Literature Review

2.1. Tantalum

Tantalum is a semi-precious, refractory metal with a high melting point at 3269K, high wear and chemical resistance. Pure bulk tantalum typically forms the ductile alpha phase, bcc crystal structure, with cell parameter of 0.33058 nm. This structure has resistivity ranging from 15 to 60 μΩ cm. When tantalum is deposited as a thin film, however, it forms a hard and brittle tetragonal structure with bulk resistivity of 170–210 μΩ cm [1]. This beta phase tantalum is metastable and will completely transform into alpha phase upon heating to temperature of 1023–1048K [2]; phase transformation begins at 573K. Beta phase tantalum is usually created as thin films by magnetron sputtering, chemical vapor deposition, or electrochemical deposition.

Tantalum has an electron configuration of [Xe] $4f^{14}$ $5d^3$ $6s^2$. It reacts readily with oxygen to form a protective oxide layer on its surfaces when exposed to atmosphere. This layer of tantalum pentoxide is stable and will resist the effects of many corrosive agents.

In microfabrication the formation of this layer of oxide and incorporation of impurities during and after deposition causes typical film resistivity to rise above the bulk value by orders of magnitude. Due to tantalum's high melting point, the homologous temperature during room temperature deposition is low enough for columnar structures to be the dominant constituent in film. This causes the density of the film to decrease and allow atmospheric oxygen to penetrate the

film. Since tantalum oxidizes readily a native oxide layer would form on any exposed surfaces, including the gaps between the columns. Thus, to improve the stability and lower resistivity of the film, tantalum films are usually annealed in an inert atmosphere to the point of re-crystallization during or after deposition [3].

A common method of producing tantalum nitride and tantalum pentoxide is sputtering tantalum in the presence of reactive gases such as nitrogen and oxygen. This method of production can produce a wide range of stoichiometries and film morphologies depending on process parameters such as base pressure, working pressure, RF power, voltage bias, temperature of the substrate, and partial pressure of the reactant gas [4].

2.2. Tantalum Nitride

Tantalum nitride had been used as an anti-corrosion coating in steel works, diffusion barriers for copper interconnects, and surface mount resistors. Methods for depositing tantalum nitride include electron beam evaporation, dc diode reactive sputtering, planar magnetron reactive sputtering, chemical vapour deposition, RF magnetron sputtering, and atomic layer deposition. Tantalum nitride has a bulk resistivity of 252 μΩ cm. However due to differences in composition and morphology, tantalum nitride thin films often have very different resistivities. For example, in the works of Riekkinen [5], it was identified that the progressive transformation from β-Ta, Ta_2N (5% N -flow), to hexagonal TaN (10% N -flow) and f.c.c.-TaN (15% N -flow) gives resistivity values of 166 μΩ cm, 234 μΩ cm, 505 μΩ cm and 531 μΩcm, respectively. In Figure 2.1, we see

the transition between different tantalum nitride phases with increasing nitrogen atomic percentage.

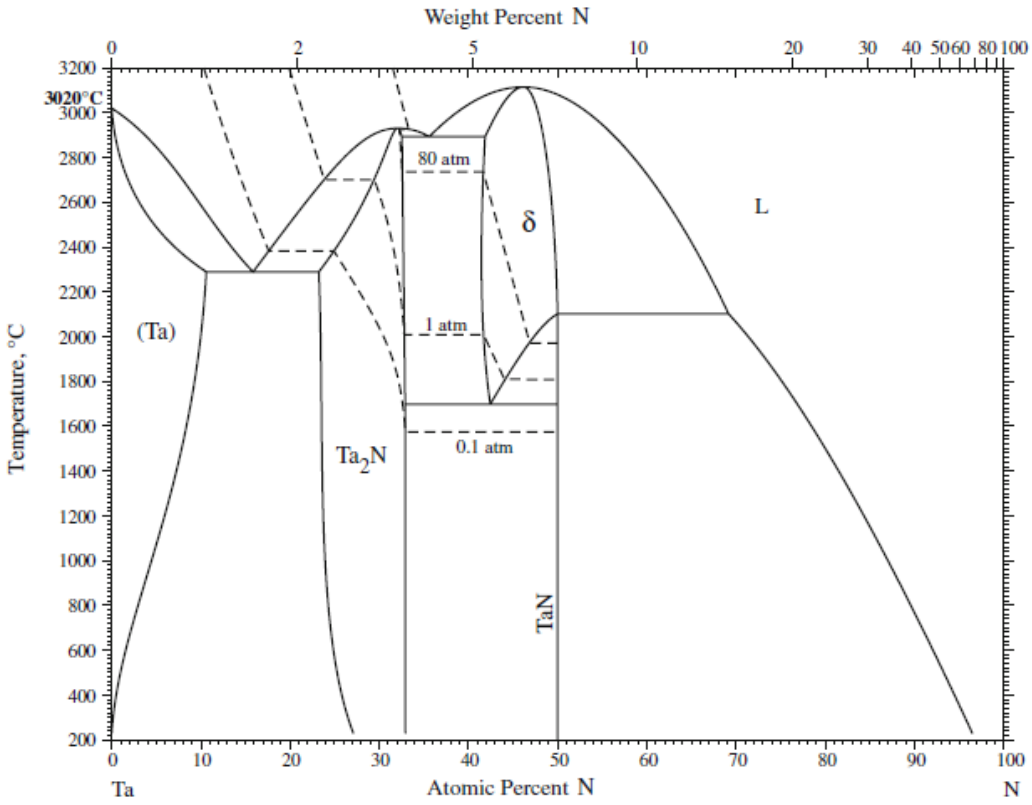

Figure 2.1 Tantalum Nitrogen Phase Diagram[6]

Comparing the above phase diagram with the resistivity of tantalum nitride films deposited by RF magnetron sputtering in Figure 2.2, it can be seen that the resistivity of sputtered films depends significantly on its phase composition. Sputtering tantalum nitride films under the same parameters often create very different film properties because of small variations in chamber conditions. Common methods for reducing and stabilizing resistor values are annealing and laser trimming, which can be done after deposition or during device fabrication.

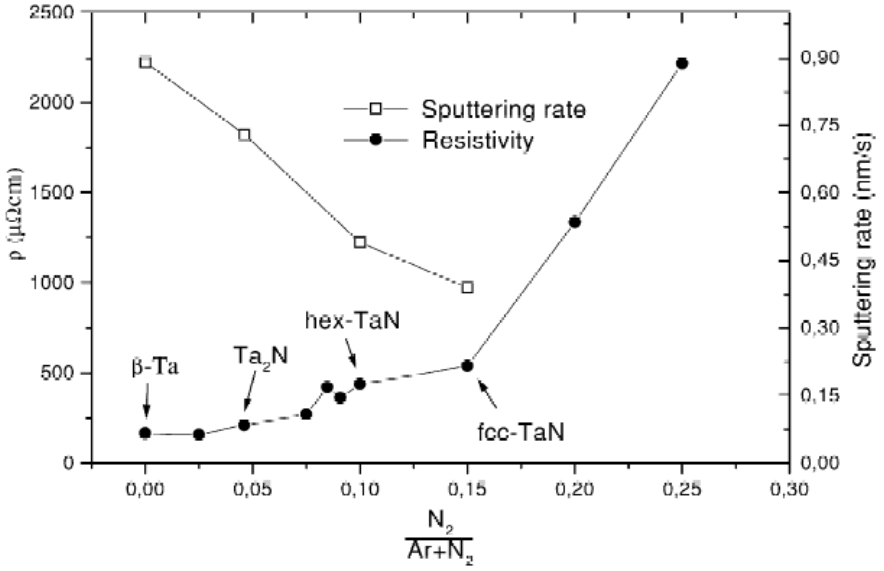

Figure 2.2 Deposition rate and Phase of Tantalum nitride in RF Magnetron Sputtering [5]

From the works such as Sun[7], it is known that the composition of tantalum nitride can range from 0 to 60 % nitrogen. Conductivity of tantalum nitrides vary from metallic in nitrogen deficient films to insulating super-stoichiometric films depending on the nitrogen partial pressure during deposition. The progression is paralleled with the transition from bcc-Ta to Ta_2N, then to TaN, and finally to Ta_5N_6 as the film reaches nitrogen saturation at 60 % nitrogen. Other phases with higher nitrogen to tantalum ratio have been mentioned in the work by Stampfl [8], along with the electronic properties of stable and metastable forms of tantalum nitride. Atomic densities of sputtered films initially increase with nitrogen partial pressure and then decreases as nitrogen content continues to increase. For deposition at temperature below 873K, the resultant film is typically amorphous. Annealing the films in temperatures above 973K crystallizes tantalum nitride into

hcp grains and is typically used in the industry to stabilize resistor values. As the melting point of this compound is 3573K [9], tantalum nitride has a high thermal stability and is generally used by microelectronics industry as a diffusion barrier between copper and silicon.

Characteristics that make tantalum nitride a preferable electronic material are: low temperature coefficient of resistivity, thermal stability under high temperatures, chemical stability, and a wide range of conductivity values. These properties allow the design and fabrication of extremely reliable and temperature stable thin film resistors. These resistors would serve as a part of an external circuit used for measuring the pH response of the ion conductor. The parameters for producing specific resistivity in tantalum nitride films are specified in work by Kang [10], which states for nitrogen partial pressures of 10.5 to 20.6% in a total chamber pressure of 0.7 Pa, film resistivity is relatively constant. He had also identified his films as mostly stoichiometric tantalum nitride in this stable region.

2.3. Tantalum oxide

Tantalum pentoxide is a high K dielectric commonly used in capacitors, antireflective coatings on lenses, and solid state fast ion conductors. It is potentially applicable as the ion conductor for fuel cells and microfluidic devices. Dielectric constants of tantalum pentoxide have been reported as high as above 20 depending on the fabrication process and parameters [11]. The melting temperature of this material is reported at 2145K. The bulk density is at 8.2g/cm^3. Methods for producing tantalum pentoxide film includes: anodic or thermal

oxidation of physically sputtered Ta, reactive sputtering of tantalum, direct/assisted CVD, oxide sputtering, vacuum evaporation, Sol-gel methods, ALD, and Ion assisted deposition. The ion conductivity of the tantalum oxide can be enhanced by increasing the porosity of the film through high deposition pressure [12]. A phase diagram of Ta-O system can be seen in Figure 2.3.

In the reactive sputtering of tantalum in plasmas of argon and oxygen, oxygen dissolves in tantalum readily and stays in solution until oxygen reaches a maximum 4.9 atomic % (at 1823K+/-30K) or lower (for lower temperatures), as shown in Figure 2.3. Additional oxygen will begin to form the compound of tantalum pentoxide, which is composed of tantalum and oxygen at ratio of 2:5, with tantalum and its oxide forming a composite.

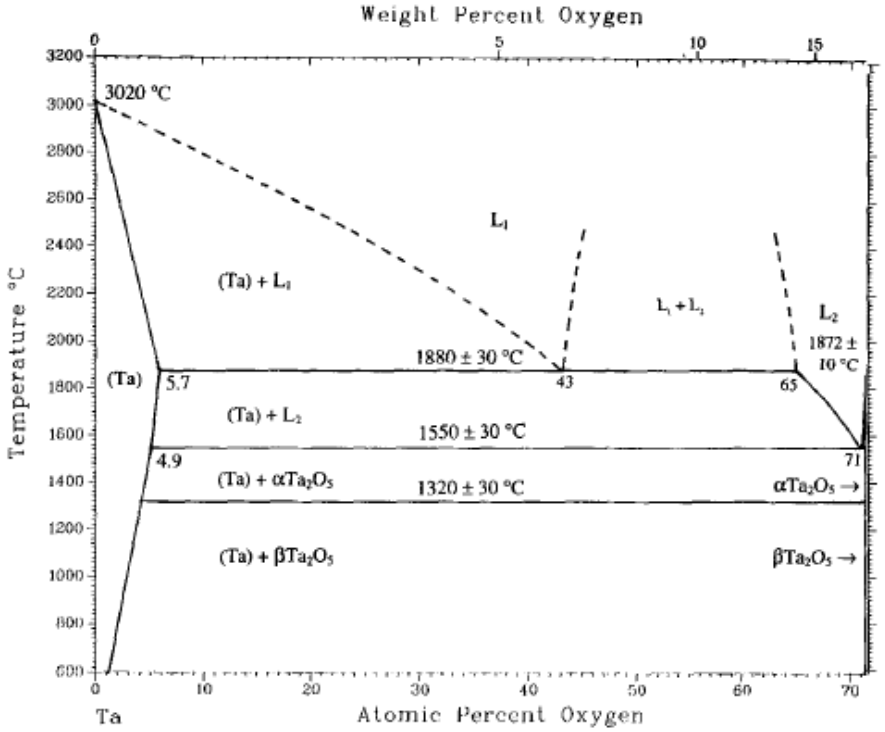

Figure 2.3 Tantalum-Oxygen phase diagram [13]

The most stable oxidation state of Ta is +5 in Ta_2O_5, but other oxidation states such as +4 in TaO_2 are also reported in work by Wang [14]. The structure of tantalum pentoxide films is dependent upon its process temperatures. At temperature above 973K, the film transforms into a polycrystalline film with either orthorhombic or hexagonal lattice structure. Orthorhombic tantalum pentoxide has a high temperature and a low temperature form with a reversible transition temperature at 1633K, as summerized by C. Chaneliere[11].

At deposition temperatures below 923K, the tantalum pentoxide retains an amorphous film structure. The composition of reactively sputtered tantalum pentoxide films varies with oxygen partial pressure and can be divided into two broad ranges. When oxygen partial pressure is low, oxidation occurs primarily at the substrate with tantalum adatoms reacting with absorbed oxygen atoms at the surface. As oxygen partial pressure increases, the ratio of oxygen to tantalum increases until the surface of the substrate is saturated with oxygen. Further increases in oxygen partial pressure will not increase the oxygen to tantalum ratio since the additional oxygen will not absorb onto the substrate surface and react with tantalum adatoms. For high partial oxygen pressures, the primary site of oxidation is at the target surface. It was proposed that molecules of tantalum oxide are desorbed from the target surface under ion bombardment. The molecules are then deposited onto the substrate surface where it incorporates the extra oxygen needed to make the film stoichiometric tantalum pentoxide.

The effect of oxygen partial pressure on the stoichiometry of tantalum oxide films is documented in a paper by Chen[15]. In the paper, films are deposited using a CVC AS601 Model dc magnetron sputtering system. A cryo pump reduces the base pressure 26.7 μPa. The planar magnetron sputtering cathode was at the bottom base plate, which consisted of a sputter target, magnets, and cooling plate. The target used was a 20.32 cm diameter, 0.635 cm thick Ta plate with 99.95% purity. Attached to the bottom of the cylindrical system was a rotary holder with ten substrate positions for 12.7 cm Si wafers. The substrate holder was about 5 cm above the Ta target and was connected to the ground of the power supply. The substrates were rotated into position over the deposition target during deposition at a speed of 20 RPM. Commercial grade argon and oxygen gases were introduced through two gas lines and mixed together before being introduced into the chamber. The flow rates of Ar and O_2 were separately controlled through mass flow controllers.

During deposition, the chamber was first backfilled with Ar gas and used to sputter clean the Ta target for at least 5 min. Then the Ar/O_2 gases were introduced into the chamber to reach a total pressure of 0.667 Pa. Plasma power was set at 2.6 kW, with no substrate heating or cooling, and the argon to oxygen ratio varied as the control variable. Argon flow rate was generally fixed at 80 sccm, except during deposition with 100% oxygen plasma.

In the above reference, a stoichiometric film was produced as the flow rate of oxygen reached 35 sccm. The peak target voltage was reached at 30sccm,

however to achieve reproducible and good quality oxide the oxygen flow rate had to exceed the above point. In the former case, the resistivity and the stoichiometry depended on the oxygen partial pressure in the chamber. In the latter case the stoichiometry and resistivity of the film were not dependent on oxygen partial pressure due to the saturation of surface oxygen on both the substrate and tantalum target surfaces. XPS measurements indicate that during argon sputtering of the sample surfaces oxygen was preferentially sputtered, which lead to a gradual reduction of O/Ta ratio in their data.

The bandgap of tantalum oxide ranged from 4.3 eV for stoichiometric tantalum pentoxide in Cervo and Carter[16] to 4.0 eV for substoichiometric oxides, and then decreasied from 3 to 0 eV as the tantalum content of the film increased. C. Chaneliere[11] summarized the state of research into tantalum oxide; it was stated that amorphous tantalum pentoxide have band gaps between 4.2 to 4.4eV, while crystalline tantalum pentoxide has a wider range of band gaps from 3.9 to 4.5 eV. We can use the bandgap of the deposited film to identify its morphology.

Current causes of ion conduction in tantalum pentoxide are unclear, but evidence in literature, such as the work of Hughes[17], indicates that both the Schottky effect and Poole-Frenkel effect may be the mechanism for ion conduction. The Poole-Frenkel effect arises when the positive oxygen vacancy defects in the insulator trap electrons that are injected into the oxide, thereby preventing them from conducting. At sufficient electric field strength band bending would lower the coulomb barrier trapping the electrons and allow them to be injected into the

conduction band. The Schottky effect injects electrons from the electrode into the oxide. As the negative charge builds up in the oxide an electric field is generated across the oxide layer. This applied field forces ions Na^+ and H^+ to migrate through the film.

2.4. Ion Sensors

In biology and chemistry, the most critical information is often obtained by determining the species and concentration of ions in a solution. The measurement of pH is one specific application for ion sensors. The acidity of any given solution is measured on the pH scale, which typically corresponds to the concentration of H^+ ions in solution. Devices like the ion sensitive field effect transistor [18] (ISFET) and Beckman pH meter are two types of ion sensors.

2.5. History of pH measuring devices

The current approaches for measuring pH are done by inexpensive but relatively inaccurate litmus paper or accurate but expensive laboratory pH meters. Typical pH instruments use electro-potential of an ion selected electrode in a sample solution with respect to a reference electrode, and calculate the pH from the voltage difference. There have been efforts by various members of the academic and industrial community to produce inexpensive and reliable pH meters for in-situ-testing outside of lab environment. However, due to various issues of reference potential drift, temperature effects, and surface charge accumulation, in-field pH meters are typically an order of magnitude less accurate than their laboratory counterparts.

The pH scale was first introduced in 1909 by Danish scientist Soren P.L. Sörenson[19] for measurement of ionic dissociation in a solution. The lower pH number indicates high acidity and the high pH indicates high alkalinity. The actual quantity measured is the concentration of H^+ ion in the solution. The relation is pH equals to the negative log of the concentration of hydrogen ions.

$$pH=-\log(a_{H+})$$

a_{H+} is the activity of the hydrogen ion in units of Mol/L. Activity represents the reaction rate of an ion species in solution, its value is a constant multiplied by the concentration. When the concentration of ions is low, the activity of the hydrogen ion can be approximated as the concentration of the hydrogen ion [20]. At very high ion concentrations the activity coefficient decreases.

Neutral solutions have a pH of 7. In conventional pH meters, such as the Beckman pH meter [21], the measurement system consists of three parts: a pH measuring electrode, a reference electrode, and a high input impedance meter. The pH electrode has a voltage that varies with the pH of the measured solution. The pH measuring electrode is a hydrogen ion sensitive glass bulb. It has a millivolt output that varies with the relative hydrogen ion concentration between the inside and outside of the bulb. The reference electrode output does not vary with the activity of the hydrogen ion. The pH electrode often has a very high internal resistance, making the voltage change with pH difficult to measure. The input impedance of the pH meter and leakage resistances are therefore important factors. A high impedance amplifier is used to measure the small electrode

voltages and displays the results directly in pH units on either an analog or digital display. In some cases, voltages can also be read for special applications or for use with ion-selective or Oxidation-Reduction Potential (ORP) electrodes.

2.6. Ion sensitive field effect transistor

A second class of pH meters, the ion sensitive field effect transistors as described by Vlasov[22], are metal–oxide–semiconductor field-effect transistor with ion sensitive gate. In this method of pH measurement, the hydroxyl groups on the gate oxide may donate or accept a proton from the solution and thereby create a positive or negative oxide surface charge. The excess ions in the solution keeps the overall charge neutral; however, this creates a two layer charge structure that can be accurately described by the Chapman-Stern model for double-layer capacitance of a series network of a Helmholz-layer capacitance (the Stein capacitance) and the diffuse-layer capacitance. The electric field from these charges controls the channel depth of the transistor and therefore the size of the drain-source current.

Because the channel depth is controlled by the charge on the gate, a key issue with Ion Sensitive Field Effect Transistor (ISFET) is the selectivity between the target ion species versus the contribution of other ion species. Due to the fact that the most vital portion of the device is in close contact with the samples, corrosion resistivity of the gate material would also be a concern. ISFETs are also sensitive to temperature changes, leakage currents, and interactions between the semiconductor and gate oxide. Getting reproducible results from ISFETs requires

tight control of environmental factors which is not available in field environment use.

2.7. Ion conductors

Ionic conduction in solids has been a subject of interest as early as the beginning of the 19th century. It was established by Michael Faraday in 1839 that the laws of electrolysis are also obeyed in ionic solids like PbF_2 and Ag_2S. Soon alpha-phases of various materials such as Ag_2S, Ag_2Se, and Ag_2Te were discovered by Tubandt[23]. By the early 1930s, it was demonstrated that these fast ionically conducting solids could be treated entirely the same as aqueous electrolytes from the viewpoint of chemical reactions and thermodynamics; hence these materials were termed solid electrolytes. Ion conductors may conduct different species of ions depending on their structure and components.

Various models which simulate ion transfer through amorphous oxide have been proposed in the literature; they include the Diagnam, the original and the modified Bean, Fisher, and Vermilyea models [24]. In the latter three, ion concentration is field dependent. They propose that metal ions are displaced from their lattice position by ordinary field-assisted thermal activation. Each displacement event would generate a vacancy and an interstitial ion, i.e. a Frenkel defect. It is assumed in these models that the negatively charged vacancies will be stationary and the positively charged interstitials will be mobile. Interstitials would be neutralized through recombination with vacancies. The generation and neutralization of these charge pairs keep the ion concentration constant for any

given electrostatic field. However, these models lack mechanisms for generating new defects in the oxide and predict that as the oxide polarizes the interstitial concentration would go through a gradual transition between the old and the new equilibrium interstitial concentration. The transient phenomena are reviewed by the work of L. Young[25], who promotes the Diagnam model of ion conduction as the most accurate, due to its explanation of how new Frenkel defects are generated via momentum transfer to mobile ions.

The Diagnam model assumes the formation of new vacancies and interstitials are due to the acceleration and collisions of charge carriers in the polarized oxide. result The build up to equilibrium state is not only a function of the field strength but also of the ion current density. In a variation of the Diagnam model, the channel model, ions travel through channels in the porous atomic structures of the amorphous films. Due to the randomness of the structure some parts will contain deeper potential energy wells that may act as traps. If these traps may be represented as coulombic, then following the well known derivation for field-assisted thermally activated release of electrons from traps (Poole-Frenkel law) we expect a steady state current density:

$$J = J_o \exp (- (W - \gamma E^{1/2}) / kT)$$

where J_o, W, and γ are constants. E is the electric field strength. Interstitial ions are expected to move along paths of least resistance. Mobile ions accelerated by the electric field transfer their momentum to stationary ions in their pathway.

These collisions may unblock additional channels and increase the current density.

$$J=B(E,T)\,\theta$$

where E is the electric field applied across the oxide and T is the temperature. The build up of ion currents density is proportional to the fraction of unblocked channels, θ.

Solid electrolytes conduct due to the movement of ions through empty crystallographic positions in their crystal lattice structure. The most commonly used solid electrolyte is yttria-stabilized zirconia, YSZ. One component of the structure, the cation or anion, in the case of YSZ O^{2-} is essentially free to move throughout the structure, acting as charge carrier. Proton can rapidly transfer charge carriers, such as hydrogen ions, through its surface space-charge layer and interstitial lattice sites[26].

Fast ion conductors are a subset of solid electrolytes. Such materials are intermediate in nature between crystalline solids which possess a regular structure with immobile ions, and liquid electrolytes which have no regular structure and mobile ions. Such materials are use in all solid state supercapacitors, batteries, fuel cells, and in various kinds of chemical sensors. A defining feature of fast ionic conduction is the existence of a surface space-charge layer on the ionic crystals which enables rapid transfer of ions. Such conduction was first predicted by Lehovec[26]. As a space-charge layer has nanometer thickness, the effect is

directly related to nanoionics (nanoionics-I). Lehovec's effect has given a basis for the creation of nanomaterials for portable lithium batteries and fuel cells.

The surface space-charge layer is a region where the mobile charge carriers have been forced to diffuse away. In this region the increase of conductivity can reach up to 10^8 times as much as the bulk material due to ion movements through inter-crystalline voids or empty crystallographic positions. By increasing the porosity of tantalum pentoxide the number of pathways available for the action of surface space-charge layer increases. Ion conducting tantalum pentoxide films have been fabricated using spin coating, physical vapor deposition, chemical vapor deposition, and electrolysis of tantalum films in aqueous oxidizer. It was observed in work of Duggan[27], Saito and Niwa[28], the minimum ionic resistivity coincides with the transitional point between opaque tantalum films and transparent oxide films. This may indicate that oxygen vacancies contribute to the rapid diffusion of ions. The index of refraction was reported in work by K. Chen[16] to be 2.07 and the dielectric constant as 20. These values were calculated from Variable Angle Spectroscopic Ellipsometry (VASE) measurements on films deposited on glass and on (100) silicon wafers. The method by which they achieved stoichiometric oxide films was to pre-oxidize the target prior to deposition. By locating the transition region where the rate of deposition and full oxidation could be simultaneously achieved, they could maintain a high deposition rate without compromising film properties.

2.8. Tantalum Pentoxide as pH sensing layer

There have been attempts to integrate tantalum pentoxide as part of various pH sensors. The most common use for Ta_2O_5 is in the gate of an ISFET or in electrode-oxide-semiconductor structures. There are several works that studied how properties like porosity and roughness of the films contributed significantly to the pH response of the finished devices. In the works of J. Chou[29], the investigators varied the working pressure, which in turn changed the roughness of tantalum pentoxide film. With decreasing working pressure and increasing film roughness, the pH sensitivity of the device increased. Effects of film porosity on ion conduction of tantalum pentoxide were covered in the work of K. Tajima[12]; an optimal film density for hydrogen ion conduction was $3.8 g/cm^3$. The effects of process temperature on tantalum pentoxide were seen in the review paper of C. Chaneliere[11] which indicated that pH response of the oxide film decreased rapidly with increasing maximum annealing temperature due to recrystallization of the film.

2.9. Sputtering

Properties of sputtered nitrides and oxides are dependent upon final film structure and composition. Therefore, it is important to examine the factors in the fabrication process which affects film composition and morphology. It is often very difficult to reproduce films deposited by DC magnetron reactive sputtering due to differences in chamber conditions or even process history.

Chapter 3: Experimental Procedure

Introduction

In this project, a pH sensor multilayer device was designed, fabricated and tested. Masks were designed and substrates were prepared; thin metallic films were deposited by DC magnetron sputtering, oxides and nitrides by pulsed DC magnetron sputtering. The resulting films were characterized; and the pH sensor was fabricated and initial tests were done.

3.1 Mask Design

Masks for patterning the devices were designed on L-Edit v14, which is dedicated mask design software from Tanner EDA. This software is a standard CAD program used in the Nanofab for designing 5”x5” photomasks. Three device designs were developed, which were replicated into four 3x5 arrays. Alignment was made along the horizontal and vertical center axes. Each layer of the mask was exported as a GDSII file to be compiled and written onto a blank chrome covered square on a Heidenberg DWL200 pattern generator. DWL200 pattern generator exposed the photo resists on the mask using multiple laser beams. The mask was then developed and etched using standard chrome etches provided by the Nanofab.

The investigator designed the mask while the compiling and fabrication of the mask was done by the Nanofab staff. Each mask was cleaned by an in house nitrogen gun prior to each use in the Nanofab.

3.2 Substrate Preparation

The substrates used in this investigation were single side polished, 100 mm diameter, 525 μm thick, N-doped Si (100) wafers purchased from Silicon Inc. Before using, the wafers were cleaned to remove all particulate and organic residues using 3 parts 96 % H_2SO_4 and 1 part 30% H_2O_2 piranha solution. The piranha solution was mixed immediately before use by pouring the H_2O_2 into the H_2SO_4 in a borosilicate glass container. The wafers were placed into the solution slowly to prevent thermal shock due to the exothermal reaction and immersed in the solution for 15 min. Afterwards, they were taken out of the solution, and excess piranha on the wafers was allowed to drip off back into the container. The wafers were then rinsed with deionised water flush. Finally, they were dried in a spin dryer with nitrogen purge. The cleaned wafers were stored in the Nanofab, until used.

Borosilicate glass slides were used to measure the deposition rates in DC magnetron sputtering. Their composition as given by the manufacturer is 70% silica, 10% boron oxide, 8% sodium oxide, 8% potassium oxide, and 1% calcium oxide. The films deposited on the slides would determine the approximate deposition rate and film resistivity for the sputtering conditions. The glass slides were cleaned before sputtering by wiping them with acetone, isopropanol, and drying them with clean room wipes.

3.3 Thin Film Deposition

Films used to fabricate the pH device were deposited via sputtering. Sputtering is done when accelerated ions produced from an inert gas plasma collides with a metal target and eject metal ad-atoms which are deposited onto a substrate. This physical vapour deposition technique is ideal for conductive metal films. However, during sputtering, reactive gases may be introduced to also deposit various compounds. One common application is the deposition of metal oxides, such as tantalum pentoxide and silicon dioxide insulators. This method was preferred over deposition from an oxide target due to its higher deposition rate.

Gases for all sputtering sessions were fed from common tanks and were regulated by digitally controlled mass flow controllers. They were mixed before injection into the sputtering chamber. The purity of the gases was recorded from the tank labels. Nitrogen used for reactive sputtering was designated UHP or 99.999 % pure, argon used was 99.998% pure, and oxygen used for reactive sputtering was 99.993% pure. A separate in house nitrogen supply (99.9%) was used for purging. Target purity and dimensions are listed in Table 3.1.

Table 3.1 Sputtering Targets Purities(7.62 cm diameter, 0.635cm thickness)

Target material	Target purity
Silicon	99.999%
Aluminum	99.99%
Chromium	99.99%
Tantalum	99.95%

The targets were in the Nanofab and were pre-sputtered in pure argon plasma before each sputtering deposition to remove contamination.

DOUG is a planar magnetron sputter system in the Nanofab. It contains three 7.62 cm diameter planar magnetron sources in co-sputter configuration, as shown in Figure 3.1. The three sources are shielded from each other and have independent shutters. They are powered by three separate DC planar magnetron power supplies, one of them is pulsed. Substrate pieces were suspended over the target on a rotating substrate holder that can hold a single 10.16cm wafer. Tooling available for holding small and irregular pieces is seen in Figure 3.2.

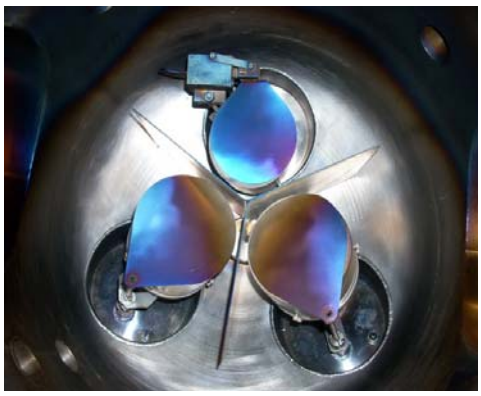

Figure 3.1: Gun configuration

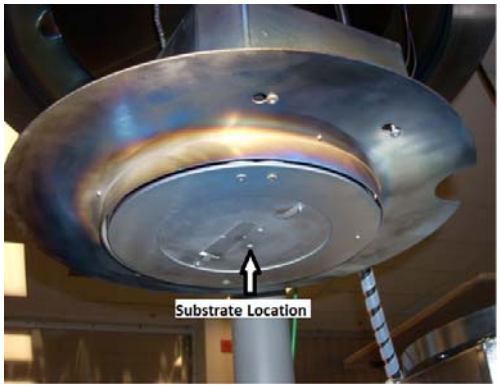

Figure 3.2: Substrate holder

Argon, Oxygen and Nitrogen feed lines entered through the back of the sputtering chamber for regular and reactive sputtering. Each gas flow rate was controlled by a mass flow controller. Sputtering gases were mixed in a common manifold before entering the chamber. The sputtering pressures were set by manual operation of the cryopump gate valve before and during sputtering. The chamber

was vented with a separate house nitrogen gas line that entered near gun 3. The substrate holder was hung from the chamber lid and was isolated electrically and thermally from the chambers walls. Views of the sputtering chamber are shown in Figures 3.3 and 3.4.

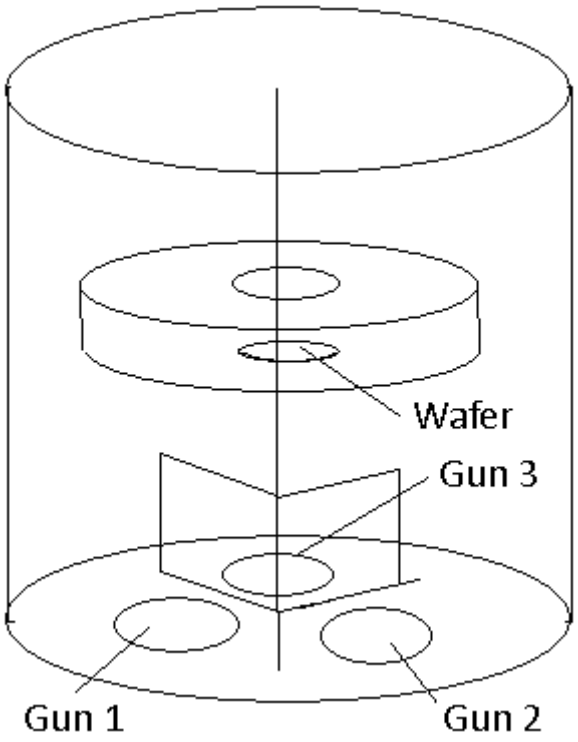

Figure 3.3: View of interior from viewport

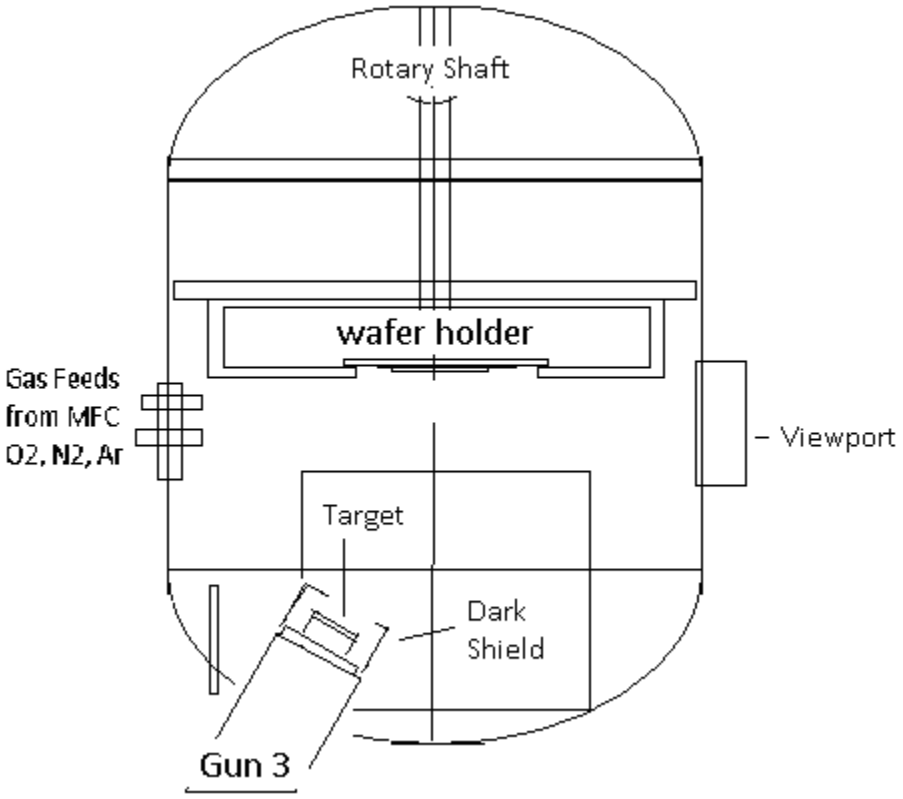

Figure 3.4: Side view seen from cryopump

These figures show the gun configuration within the sputtering chamber. The upper most sputtering source, labelled as gun 3, can sputter magnetic materials and do reactive sputtering as it has a pulse dc power supply. DOUG also has RF sputtering capability, a substrate heater for depositing at temperatures from 298K to 423K, and substrate RF bias. The sputtering chamber can be cryopumped to a base pressure of 13.33 μPa over a 48 hr interval. The regular power supplies are typically used at 300W for most metal target materials. The pulse power supply can generate a maximum bias voltage of 600V.

The left most source in Figures 3.1 and 3.3, called Gun 1, is used to sputter pure metal targets. The target to substrate distance was 14.87 cm. Gun 1 is pointed at an angle of 4.733 degrees off parallel to the vertical axis, so that the center of the Gaussian beam reaches the substrate at 5.11 cm from the center of the substrate wafer holder. The sputtering sources 1 and 2 are connected with power supplies that can generate a maximum DC power of 400W, but is typically used at 300W. For metals, such as Cr, Al, Cu, and Ti the standard sputtering power is 300W.

To make our results reproducible to others researchers, the target to substrate distances are important. In comparison with other results in the literature one can see that longer distances reduce deposition rate, but increases uniformity. Longer distances also reduce the diffusivity of the sputtered atoms due to additional molecular collisions within the chamber.

Gun 3 was used for reactive sputtering of tantalum nitride, tantalum oxide, and silicon dioxide. Target to substrate distance was 17.37 cm. The angle of the gun is pointed 6.59 degrees off parallel from the vertical axis. The center of the sputtered beam was 5.16 cm from the center of the substrate holder. A photo of the DOUG sputtering system and the alignment of Gun 3 are shown in Figure 3.5.

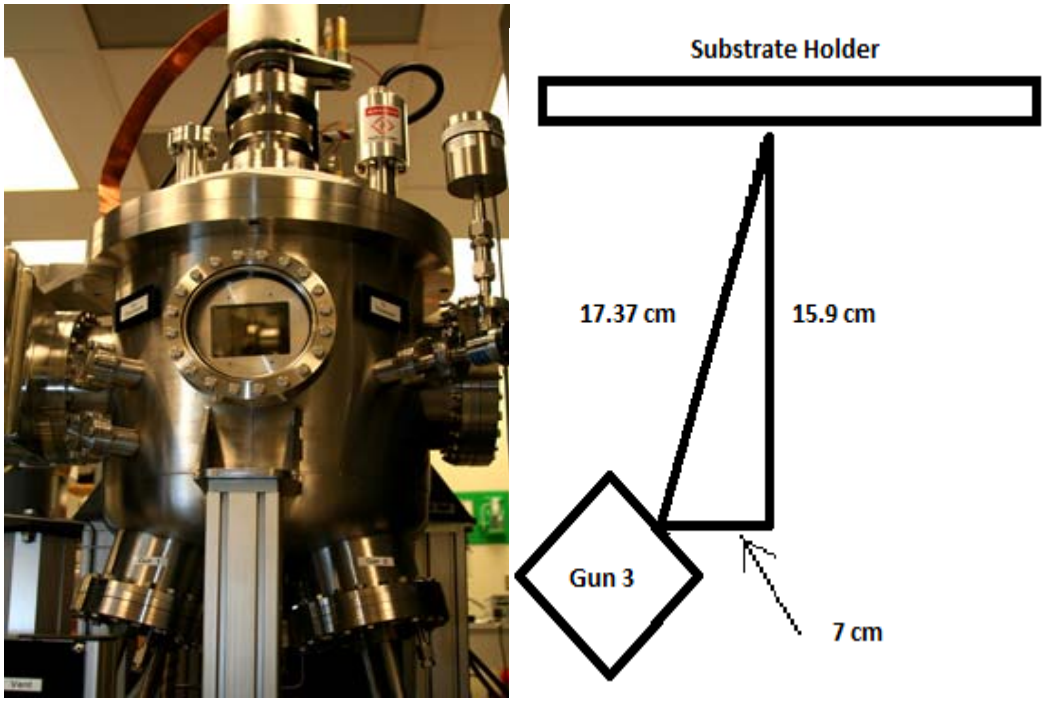

Figure 3.5: Reactive Magnetron Sputtering machine Doug and Gun 3 position

Initially, to enhance diffusion on the substrate surface, the deposition of tantalum nitride was to be done at 423 K. Substrate heating was not available, so two other methods to increase diffusion were considered. First was to lower the process pressure and second was the use of substrate biasing to increase the incident energy of the atoms. The three problems with the first approach were that the directionality of the beam increases as the mean free path decreases, the ion density would decrease as the numbers of collision between electrons and neutral species decrease, and the gas flow ratio for stoichiometric compound shifts as the deposition pressure changes. Due to these factors, if the process pressure was decreased, the non-uniformity in thickness and composition would increase and

the deposition rate would decrease. A series of deposition trials using borosilicate glass substrate were performed to determine the preferred procedure.

3.3.1 Sputtering of Metals

The sputtering of chromium backside contact was done in BOB, a separate DC magnetron sputtering machine with same internal configurations as DOU. The parameters were base pressure of 0.267 mPa, deposition pressure of 0.933 Pa. The burn time was 3 min in pure Ar at 10.5 sccm, deposition time was 15 min, and the film was allowed to cool for 10 min before extraction. The deposition time for Cr contact pads was 5 minutes using Gun 1 which produced Cr film thickness of 135 nm as measured by alphastep profilometer.

3.3.2 Ta_2O_5 Ion Conductor and TaN

The two tantalum oxide layers were deposited using DOUG, one before and one after the tantalum nitride layer. To maximize the ion conductivity of these layers, the films were made porous but continuous without further annealing. Sputtering was done with a tantalum target on gun 3 of DOUG. Base pressure before deposition of Ta_2O_5 was 3.2×10^{-4} Pa. The argon flow rate was 50 sccm. Sputtering power was set at 300W, reverse pulse time at 0.5 μs, and frequency at 150 kHz, and total pressure at 0.9333 Pa. The substrate rotation was set to 50 Hz. The target was plasma cleaned for 5 min, after which the oxygen flow rate was set to 10 sccm. The sputtering voltage stabilized after approximately 3 minutes. The thickness of Ta_2O_5 was 150 +/- 10 % within wafer, measured using marked slides and alphastep profilometer which takes five measurements across the slide.

Tantalum nitride was deposited using Gun 3 on DOUG, with fixed Argon partial flow rate of 50 sccm and nitrogen flow rate of 10 sccm. The target was plasma cleaned for 5 minutes in pure argon then with nitrogen for 3 min before deposition. Tantalum nitride was deposited on glass slides for XPS, resistance, and thickness measurements before each deposition on wafers. Deposition parameters used were sputtering power of 300 W, pulse reversal time of 0.5 μs and frequency of 150 kHz, $3.2x10^{-4}$ Pa base pressure, 0.93 Pa deposition pressure, 50 sccm of Argon, 10 sccm of nitrogen, and substrate rotation at 50 rpm. A standard deposition time of 9 minutes was used for uniform film thickness for samples on glass. Due to variations in chamber conditions, sputtering times on wafers had to be adjusted each session to produce the target sheet resistance of 50 Ω per square. The resistance of the film stabilized at 49 Ω per square with film thickness of 126nm+/- 10%.

The tantalum nitride was deposited at room temperature with no substrate bias or heating due to potential problems of Ta implantation in the oxide layer. The finished film was tested with the four point probe for sheet resistance and then underwent photolithography and ion milling.

3.4 Fabrication of Test Devices

After Cr metallization, the wafers were cooled and transferred to DOUG for reactive sputtering of tantalum pentoxide. The initial layer of tantalum nitride, a resistive metal compound, was deposited by reactive sputtering of a tantalum

metal target in plasma of argon and nitrogen. The process optimizations were described in section 3.3.2.

The most complicated mask design was done for patterning the tantalum nitride layer. For the device to function, the parallel resistor network must have closely matching resistance values. Factors affecting the resistance of the resistors were: the resistivity of the film, the thickness of the film, the length of the serpentine, the width of the serpentine, and the morphology of the film. The length and width of the serpentine were well defined and sufficiently large that errors in photolithography would be small. The resistivity of the film however was determined by its local thickness, morphology and the composition. The film thickness was controlled by varying the length of the deposition, the accuracy was within 10% of the target thickness within the wafer.

3.4.1 Photolithography and Patterning

To pattern films, we used ABM mask aligner with UV to expose HPR 504 photo resist. Contact lithography produces a sharp exposure profile within a few seconds of exposure, after which excess resist is removed with an alkaline solution. Typical exposures used 1.3 μm thick resist that was baked at 388K for 90 seconds and rehydrated for greater than 20 minutes at 293K with 40% humidity. Luminosity of the lamp at 365nm wavelength was 14.3W/cm^2 on average with non-uniformity of 1.7%, while at 400nm wavelength it was 47.5W/cm^2 with non-uniformity of 1.3%. The exposure factor on the machine is 0.8804. The exposure was set at 2.1 seconds.

After exposure, the wafers were placed in a pan of 354 developer(a sodium hydroxide solution) for 20 seconds to dissolve the exposed resists. The wafers were removed from the pan and rinsed for 1 minute with deionized water. The wafers were blow dried with a nitrogen gun and inspected with an optical microscope for defects such as device dimensions.

Oxford Ion Fab 300+ was used to pattern the resistors by ion milling. This equipment uses a beam of argon ions to sputter etch exposed material from the surface of the wafer. It uses RF power to dissociate argon into ions. Substrate rotation was 20 rpm. The process idles for 4 min for every 1 min etch cycle to reduce baking of the resist.

Ar ions are accelerated to energies of 180 eV using a grid to form a highly direction beam. By setting the beam normal to the wafer surface, the ions transfer the photo resist pattern onto the tantalum nitride layer through sputtering of the exposed areas. Vias through tantalum oxide were fabricated using the same procedure as above. The process is anisotropic and non-selective, so measurement on the thickness of the tantalum oxide film must be taken before and then via depth after each etch session to ensure proper etch time. The majority of photoresist was removed by an ultrasonic bath in acetone, and then the rest was removed by oxygen plasma etch.

3.4.2 Liftoff process and Ashing

Electrodes of the devices were fabricated using photo resist via mask to liftoff excess metal from the surface of the wafer. This technique involved sputtering

the metal on top of the remaining masking layer for the vias and then dissolving the remaining resist with acetone. Due to the deposition and ion milling processes, the surface of the photoresist is usually hard and resists dissolution. After using acetone to remove the majority of the excess metal the wafer was placed into as oxygen plasma RIE system where the residual resist was burned off.

The resistors were designed with matching resistances as part of an external circuitry for the purpose of measuring small voltage differences.

3.4.3 Silicon dioxide barrier layer

A thick layer of oxide is required to isolate the reference resistor from the test solution. The deposition of the oxide was done by magnetron sputtering of silicon in the presence of oxygen using Gun 3 of DOUG. The wafer rotation was set to 50 Hz. The silicon target was presputtered for 5 min with pressure at 0.93 Pa, Argon flow rate at 50 sccm, DC power at 200W, reverse bia period of 0.5 seconds, and reverse bias frequency of 150kHz. After the cleaning period, the flow rate was adjusted to 50sccm Argon and 2.5 sccm oxygen, and chamber pressure maintained at 0.9333 Pa. The target was burned in for 3 minutes before the shutter was opened. The sputtering rate was measured from a 10 minute deposition on a glass slide, which was calculated to be 10.5nm/min. The final deposition time for 800 nm of insulating oxide was 80 min. A standard silicon dioxide etch recipe using SF_6 +CF_4 plasma was run on STS RIE etcher to etch the

800 nm silicon oxide film. The masking layer was then removed using acetone in an ultrasonic bath.

3.5 Analytical methods

The quality control of the films was key to producing a functional device. For this purpose various measuring techniques were used to find and identify key film parameters such as film thickness, resistivity, and optical responses.

3.5.1 Film Thickness Measurements

To produce a functional device, the thickness of each functional layer would have to be known and controlled. Two separate methods were used, the Alpha step profilometer for measuring thickness of chromium, tantalum nitride, and tantalum pentoxide, and the filmetric for the thickness of silicon dioxide. After each films thickness was determined photolithography could be used to pattern resistors, vias, and open trenches.

Thicknesses of the Cr layer and the Tantalum compound films were measured using the alpha step profilometer. Before the deposition of each device layer, a glass slide or quarter Si wafer underwent deposition using the same parameters as those of the actual films. This was to assess the deposition rate and film thickness and quality of the film.

There was difficulty in measuring the actual thickness of the silicon dioxide film on the device wafers, since the film was deposited on top of various structures

that could be damaged by production of measurement vias by liftoff. Therefore an alternative method was used; Filmetrics measurements were done first on the tantalum oxide before the deposition and then on the Ta_2O_5+SiO_2 combined thickness after deposition, and thereby calculating the SiO_2 thickness by subtraction.

3.5.3 Resistance Measurements

In order for the final device to work properly, the resistance of the tantalum nitride film would have to be stable and repeatable. For this purpose, a four point probe as seen in Figure 3.6 was used to measure the sheet resistance of tantalum nitride films deposited on silicon wafers and glass slides. The multimeter shown in the figure was set to four point mode, with resistance range set on automatic. The samples were placed with their center beneath the probe tips. The arm height of the probes was set to retract by 1/3 when the arm is at down position. This device then sends a fixed current through the two outer probes and then measures the voltage through the inner two probes.

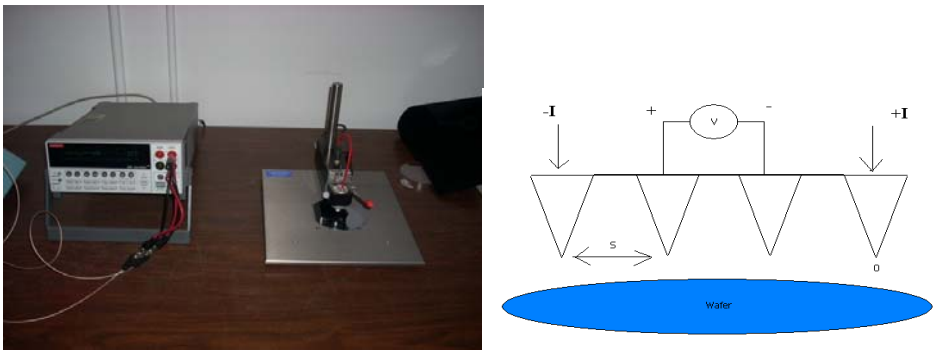

Fig 3.6: Working schematic of a four point probe.

The four point probe is used for measuring surface and bulk resistance of thin films and substrates. However, it will only measure low to moderate resistivity (1-10 Ω-cm max). The probe consists of four equally spaced tungsten tips. Each tip is set in a spring to reduce the amount of damage caused by pressing the probes onto the film. The probes were attached to an auto mechanical arm that would travel up and down when the lever arm on top of the machine is turned. During measurement, a current is supplied through the two outer probes via a high impedance current source. A volt meter then measures the voltage between the two inner probes to determine the resistivity. The tips were spaced ~1mm apart. The sheet resistance and the film thickness measurements were used to calculate the resistivity of the tantalum thin film.

3.5.3 Optical Constant Measurements by Spectroscopic Ellipsometry

Ion conduction in tantalum oxide thin films was well linked to their stoichiometry and morphology in literature. Ellipsometry is an optical measurement technique that measures the reflectance, transmittance, and changes in phase which could be used to identify the morphology and other properties of thin transparent films. This method was used to identify whether the deposition method was valid in producing tantalum pentoxide with desired film properties.

The Variable Angle Spectroscopic Ellipsometry, VASE, is an accurate and versatile ellipsometer for measuring optical properties of semiconductors, dielectrics, polymers, metals, and multi-layers. It combines high accuracy and precision with a wide spectral range up to 300to 1700nm. The instrument uses

fiber optics to transfer a beam of light to the monochromator, which selectively transmits the specified wavelength of radiation. The default beam diameter is 0.3cm, but focusing probes were available to reduce the spot size to 200um. Calibration was done with and SiO_2 thin film on Si wafer provided by the Nanofab. Alignment was performed for each sample before scanning.

The transmittance, reflectance, and absorbance of the each sample was measured. To analyze the properties of the film, we used WVASE32 modeling software to construct the expected optical response of the material and then fit it to the measurements by allowing the software to adjust the thickness and optical constants.

Tantalum and tantalum oxide films, 250 to 300nm thick, were deposited on microscope slides for VASE analysis. An R/T scan was performed over the 300 to 1700 nm range with respect to the initial reference measurement. The scans were done with beam in normal incident angle to the substrate surface. The process was repeated for all TaO samples with 0, 2, 5, 7.5 and 10 sccm oxygen flow.

3.5.4 X-ray Photoemission Spectroscopy (XPS)

XPS was used to measure the composition of tantalum nitride and tantalum pentoxide thin films. These measurements provide verification for the stoichiometry of tantalum pentoxide and tantalum nitride. Film composition was used to investigate the effects of reactive gas concentration on the final films.

The XPS measurements were performed on AXIS 165 spectrometer (Kratos Analytical) at the Alberta Centre for Surface Engineering and Science (ACSES), University of Alberta. The base pressure in the analytical chamber was lower than 3 x 10^{-8} Pa. Monochromated Al Kα (hν = 1486.6 eV) were used at a power of 210 W. Samples were cleaned in-situ by 4 keV argon ion-beam etching of area ~ 1.5 x 1.5 mm^2 for 3-5 minutes.

The analyser was run in FAT (Fixed Analyser Transmission). The resolution function of the instrument was determined to be 0.55 eV for Ag 3d and 0.70 eV for Au 4f peaks. The analysis spot was 700 x 400 μm. Electron flooding from a charge neutralizer was used to compensate sample charging during the measurements. All survey scans spanned from 1100 to 0 eV binding energy and were collected with analyzer set at pass energy (PE) of 160 eV with a step of 0.35 eV. For the high-resolution spectra the pass-energy was 20 eV with a step of 0.1 eV. Samples of TaN and TaO with various reactive gas flows were sampled with respect to sequential series of argon beam etches of 0, 3, 5, and 7 minutes. Composition was measured using O1s, Ta4f, and N1s peaks.

3.6 Measurement of Resistor Network And Devices

3.6.1 Testing of the Resistor network

Several measurements were required for initial device evaluation. The parallel resistors were measured to ensure their equivalence. The test circuits were checked for short circuits, and initial pH testing was done with standard pH solutions. Testing was done on a Wentworth probestation, shown in Figure 3.7.

To test the resistor network, a fixed current was passed through each of the parallel resistors and the voltages compared. This is shown in the Top-Down circuit in Figure 3.8 as the voltages over E->C and A->C. A Keithley 2400 current source was used for measuring the resistance values.

Figure 3.7: Device Test Rig with Keithley 2400 Source

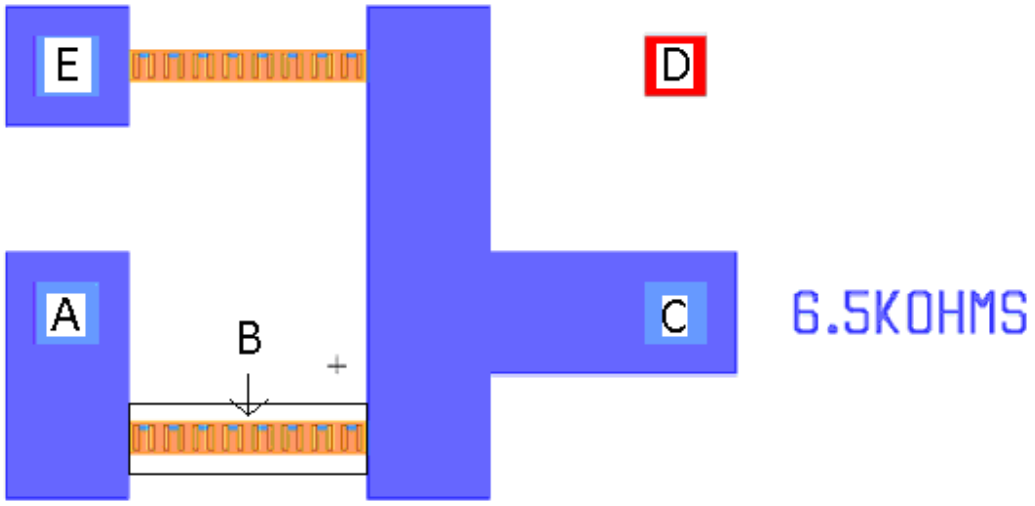

Figure 3.8: Top-Down Device Layout and Terminal Positions

3.6.2 Backside Contact measurements

To ensure that circuit shorting had not occurred during fabrication steps the voltage was measured between terminals A and D. Overload voltage due to intact insulators would signal a functional device. Again the Keithley 2400 current source was used.

3.6.3 pH testing

A schematic cross section of the pH device is shown in Figure 3.9. The wafer was washed with DI water before and after measurements. Buffer solutions with set pH values 4, 6, and 8 were used to calibrate the devices and to verify that the device is responding to the presence of solutions and its pH. The Keithley 2400 current source was set in two probe mode with auto range calibration. A micro

pipet was used to deposit 250 µL of pH buffer onto holding wells on top of the devices well B, see Figure 3.8 and Figure 3.9 terminal B.

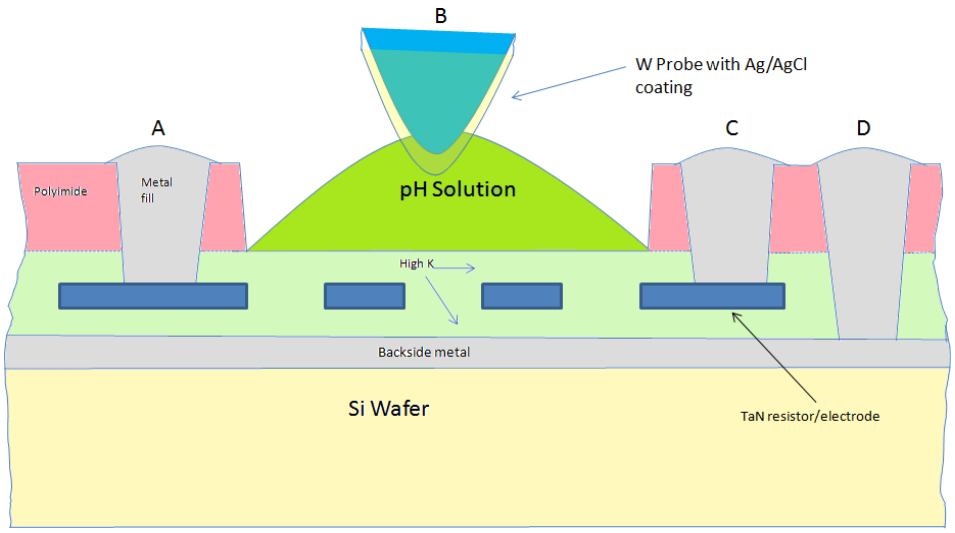

Figure 3.9: Schematic cross-section of the pH device.

A processed wafer was cleaned with deionized water before and after pH solution testing. Standard buffer solutions of Potassium Biphthalate Buffer pH 4, Potassium Phosphate Monobasic-Sodium Hydroxide Buffer pH 6, pH 7.4, and pH 8, and Potassium Carbonate-potassium borate-potassium hydroxide buffer pH 10 were used for calibration and to verify the devices' response. The pH values were given and certified by Fisher Scientific. In Figure 3.9 a schematic cross section of each device is shown using the same labelling as that in Figure 3.8. A micropipette was used to deposit a drop of pH buffer solution into the holding wells, B, of each device tested. A constant current was applied between the test probe in the test solution B and the backside contact D. The voltage was measured, resistance calculated. The circuit was reversed to determine if the

device was directional in nature. This was repeated for all pH solutions. All tests were performed at 295K.

Chapter 4: Experimental Results and Discussions

4.1.Selection of Materials

A functioning pH meter needs compatible contact, insulator and resistor materials that can function in acidic and basic environments. Therefore, the dielectric constant and ion conductivity of the oxides, resistivity and availability of the targets, and process compatibility for fabricating each device layer are the decisive factors in what metals and oxides are used in the device.

4.2.Selection of electrodes

In microfabrication, the typical interconnects between device elements are made of aluminum, copper, or gold due to their high conductivity. Other metals that are used are chromium, silver, tungsten, and tantalum. However, due to the corrosive working environment and the material and process limitation, only a few metals can be used in fabrication.

For design purposes, the key criteria for conductor layer and electrode materials are: conductivity, material and processing compatibility, corrosion resistance, and diffusivity with respect to other layers. Considerations on conductivity arose when we obtained metallic film resistance many times greater than bulk values. After investigation by Can Xu[30], it was determined that the increase in film resistivity was due to the relatively high working pressure and low substrate temperature used in the deposition processes. The bulk resistivity and melting temperature of the candidate materials are listed in Table 4.1.

Table 4.1 Metal Bulk Resistivity and Melting Temperatures

Metal [33]	Bulk Resistivity (μΩ cm)	Melting Temperature (K)
Gold	2.35	1337K
Copper	1.67	1358K
Silver	1.47	1235K
Alumium	2.63	933.4K
Chromium [34]	12.6	2180K

Figure 4.1 shows a diagram of the Thornton zone model [31 with zones labelled as I, T, II, and III. These zones describe the general morphology of a sputtered film with respect to sputtering pressure and the homologous temperature. Within Zone I the atoms do not have sufficient energy to diffuse far from initial point of adsorption and therefore accumulate in porous columnar structures. As the homologous temperature increases or the pressure lowers the atoms diffuse more and form a denser fibrous structure in zone T. With higher temperatures the film enters the zone II where the atoms have sufficient energy to nucleate and form crystalline grains. In zone III, grain growth increases due to the high homologous temperature.

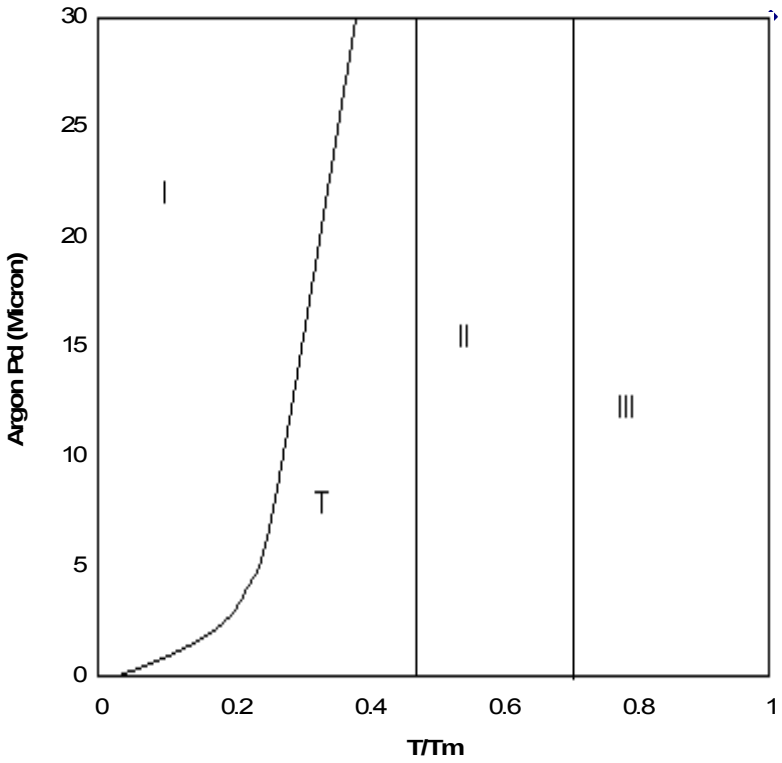

Figure 4.1 Zone Model

Magnetron deposited gold films have a bulk resistivity of 2.35 μΩ cm. The melting point of gold is at 1337K, which gives gold films sputtered at 293K a homologous temperature of 0.222. At room temperature, the homologous temperature of gold coupled with the 0.933 Pa deposition pressure would give gold films a zone T fibrous morphology. Gold contacts are chemically inert so the probability of change due to oxidation and corrosion is negligible, and therefore, resistivity of sputtered gold films is close to the bulk value. Working with gold has some disadvantages: the lack suitable etchants and gold non-adherence to silicon, thus requiring an adhesion layer of other metal such as titanium. Copper has a bulk resistivity of 1.67 μΩ cm, and a melting temperature

of 1358K: Copper, however, is well known for diffusing through both silicon and insulating oxides during high temperature processes, which would require deposition of additional diffusion barrier layers. The bulk resistivity of silver is 1.47 μΩ cm. The melting point of silver is at 1235K, which gives it a homologous temperature of 0.237 at 293K. However, PVD silver films react with oxygen to form silver oxide on exposed surfaces. Silver oxide is readily attacked by acidic solutions and therefore not suitable.

Aluminum was commonly used in early interconnects. It has a bulk resistivity of 2.5 μΩ cm, and melts at 933.4K. Aluminum reacts readily with atmospheric oxygen to form a protective oxide layer. Furthermore, aluminum is relatively easy to pattern using aluminum etches available in the Nanofab and adheres well to both silicon and tantalum compound films. In literature, multilayer films with tantalum oxide and tantalum nitride doped with aluminum indicates that aluminum reduces tantalum pentoxide to a more conductive compound. In the laboratory, contacts made from aluminum films short out tantalum pentoxide dielectric.

Figure 4.2 shows the stability of various electrode materials with respect to Ta_2O_5. In the figure, the materials are plotted with respect to the change in Gibb's free energy (ΔG) and work function. For positive ΔG the electrode is stable, while for negative ΔG the electrode would react with the Ta_2O_5. The electrode material requires a positive ΔG and low work function without affecting the structural

strength of the contact pads. Therefore, we looked at the candidates materials located on the upper left quadrant of Figure 4.2.

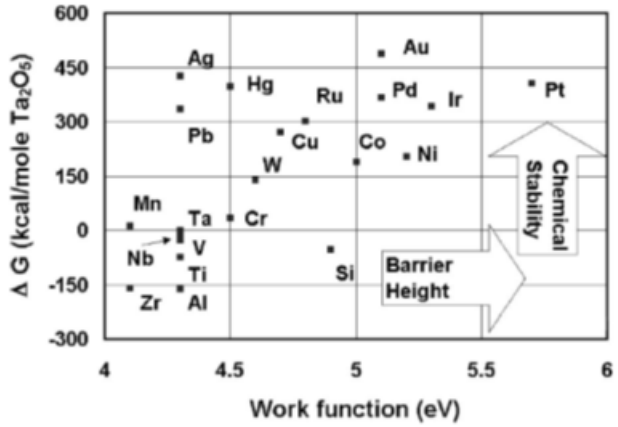

Figure 4.2 Calculated chemical stability of Ta_2O_5 with respect to potential metal electrodes [32].

Chromium has a bulk resistivity of 12.50 μΩ cm. When deposited at 0.933 Pa, chromium films have resistivity much higher than the bulk value at 243.6 μΩ cm vs 12.50 μΩ cm due to its high melting temperature at 2180K. It is stable when in contact with tantalum oxide films, but it's also expected to have resistivity many times higher than bulk value due to its low homologous temperature at 0.134.

After investigation by Xu[30], it was determined that the increase in resistivity was due to the relatively high chamber pressure used during the deposition process.

The zone model indicates the deposition of chromium under standard DOUG pressure of 0.933 Pa would cause the adatoms to form columnar islands separated by voids as in zone 1. These voids, when exposed to atmospheric oxygen would allow tantalum oxides to form on the surface of the columns and thereby increase

the resistivity of the film. Results by Xu[30] showed by lowering the deposition pressure to 0.267 Pa, the resistivity of the film drops to 78.10 μΩ cm due to the formation of a fibrous crystal structure. Chromium was selected for the electrode layer.

During device testing, it was observed that the chromium back side contact layer became irreversibly discolored after prolonged contact with test solutions when current was applied across the tantalum pentoxide layer. This indicated electrochemical reactions between ion species in solution and the chromium metal either through pin holes of the insulating film or by the reaction of diffusing ions with the metal under layer. According to the zone model, as shown in Figure 4.1, the deposition of chromium under the standard DOUG pressure of 0.93 Pa would cause the adatoms to form columnar islands separated by voids (Zone 1).

4.3. Selection of Dielectrics

Prospective oxides for both the high-k dielectric layer and the insulating layer included tantalum pentoxide, hafnium dioxide, hafnium silicate, titanium dioxide, zirconium oxide, zirconium silicate, aluminum oxide, yttrium oxide, and silicon dioxide. The criteria for oxide selection were: dielectric constant, band gap, ion conductivity, and ion selectivity.

Selecting an ion conductor for this application, the material must exhibit the following characteristics: a high dielectric constant for fast response to changes in applied voltage, a large bandgap to limit leakage currents from electron flow,

large ionic conductivity for ease of signal detection, and high ion selectivity for proton versus other ion species.

The most promising insulator for ion conduction purposes would be either titanium dioxide or tantalum pentoxide, and the ideal isolator material for devices is silicon dioxide. The form of titanium dioxide required is hydrous titanium(IV)oxide, which is not process adaptable for thin film applications, thus we focused our effort on using tantalum pentoxide and silicon dioxide. The properties of these oxides are shown in Table 4.2.

Table 4.2 Properties of Oxides

Insulators	Dielectric Constant	Band gap (eV)	Ion conductivity (S/cm) (at 25C)	Ref	primary carriers
Tantalum Pentoxide	26	4.3-4.9	10^{-5} to 10^{-10}	[32],[28], [27],[35]	H^+
Hafnium Dioxide	25	5.5–5.6	High temperature only	[36]	O^{2-}
Hafnium Silicate	25	5.5-5.9	High temperature only	[37]	H^+
Titanium Dioxide	80	2.96-3.2	$10^{-3.5}$	[38],[39]	H^+
Zirconium Oxide	25	5-7	High temperature only		O^{2-}, minor H^+
Zirconium Silicate	20	6.36	High temperature only	[40]	
Aluminum Oxide	7.5	6.4-6.8	NA	[41]	
Yttrium Oxide	15	5.5	High temperature only	[42],[43]	H^+
Silicon Dioxide	3.9	9	NA	[44]	

4.4.Effect of reactive gas flows on Tantalum Nitride films resistivity

Generally, the resistivity of metallic films increases proportionally with increasing reactive gas flow, however, in some metals such as tantalum transient behaviours are observed as different phases appear and disappear with additional nitrogen. The resistivity value for tantalum nitride increased slowly from 0 to 2 sccm, see Figure 4.3, then stabilizes in the range between 2 and 5 sccm, and increase rapidly at higher nitrogen flow. This is shown in Figure 4.3 and agrees with values and trends seen in the works of Kang[11].

The deposition rate was measured by depositing multiple films and then measuring each sample with the four point probe and alpha step profilometer. Typical film thickness varied by 10%. Stoichiometry and stability of the films varied as a function of the reactive gas to inert gas ratio. The largest change in resistivity with respect to time in atmosphere was on the films with the most amount reactive gas. However, it was observed that the films processed with flow rate of 2sccm were marginally less responsive to exposure than both films with negligible or substantial nitrogen flow. This can be explained by the formation of a eutectic system at that composition between tantalum and Ta_2N. This eutectic has a relatively higher homologous temperature than either pure tantalum or pure Ta_2N and also a higher density. The deposition of tantalum film at base pressure of 2.7×10^{-4} Pa had a resistivity range from 181.6 μΩ cm to 2044.4 μΩ cm. This was much higher than the bulk resistivity of tantalum at 13.1 μΩ cm and was dependent on the thickness of the film. The high resistivity was related to the

high melting point of tantalum at 3290K and low homologous temperature during deposition, which favoured the growth of a porous film structure. When the porous films were exposed to the atmosphere, oxygen readily oxidized the voids and diffused into the film, and increased film resistivity.

Resistivity of tantalum nitride film increased from 181.6 μΩ cm to 578.9 μΩ cm for nitrogen flow rates of 0 to 10sccm. There was a steeper increase in resistance as nitrogen flow rate increased above 10 sccm; this is shown in Figure 4.3. The resistivity values increased with the nitrogen flow rate and the deposition rate decreased as the amount of nitrogen increased. The line shows only an estimated relationship.

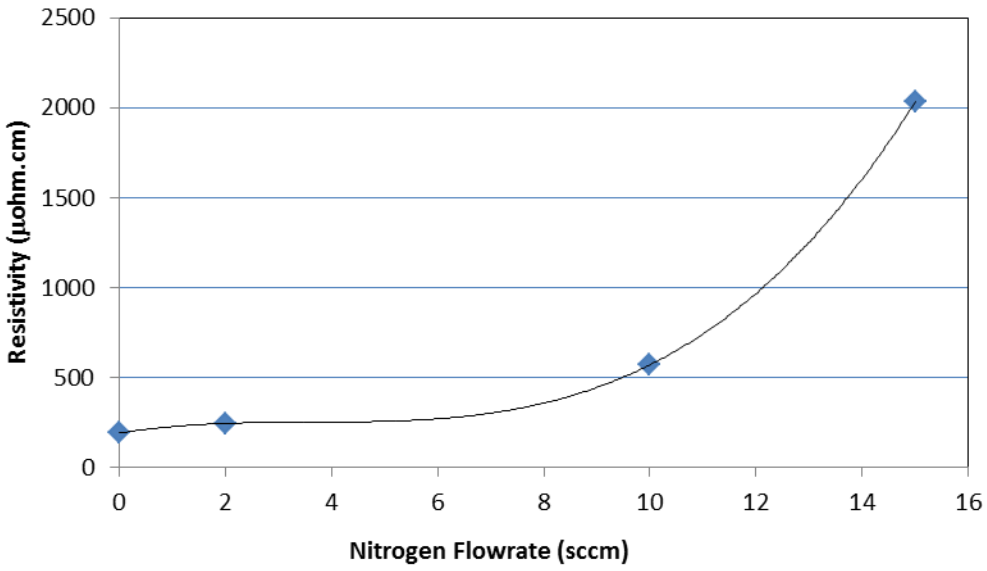

Figure 4.3 TaN resistivity as a function of nitrogen flow rate with a sputter pressure of 0.93 Pa and constant Ar flow rate of 50 sccm.

The film resistivity measured by the four point probe showed that the films deposited on silicon were more conductive than films deposited on glass. Film

resistivity varied by 10-15% and deposition rate varied by 10% when films are deposited using the same parameters. This was due to the surface roughness and charging of the substrate during deposition. The rough surface of glass slide substrate increased the effective distance between points on the film and encouraged the formation of discontinuities. On insulator films, argon ion charges accumulate and repel subsequent argon ions, so adatoms have less energy available for diffusion. According to the zone model, this effectively depressed the homologous temperature of the film and promoted the formation of a columnar film structure with more voids and thus more resistive films.

Resistance measurements showed the resistivity of pure tantalum films on glass slides increased from 181.56μΩ cm from just after deposition to 202.22 μΩ cm after 71 days. The increase in resistivity was significantly larger than values obtained from comparable works in literature which may have risen from the thickening of the native oxide within the porous film.

For tantalum nitride films deposited under various nitrogen flow rates the effect of exposure to atmospheric oxygen increased resistivity as the ratio of nitrogen to argon increased. The effect on resistivity was small from 0 to 10 sccm nitrogen, but increased above 10 sccm. This can be explained by the phase transition from semi-conducting tantalum nitride intermixed with free tantalum to stoichiometric tantalum nitride with excess nitrogen. With the phase shift the mechanism for metallic conduction was eliminated and the insulating property of super-stoichiometric TaN_y became dominant. The higher nitrogen content also

increased the effective homologous temperature of the film and produced a more porous film structure.

4.5.The effect of nitrogen on tantalum nitride deposition Rate

From literature, it was expected that as the depostion rate of tantalum nitride increased, the density of the film would decrease with increasing atomic percentage of nitrogen. At a certain point, the target surface would begin to be covered by a nitride layer and the deposition rate would decrease. Figure 4.4 shows the experimental data of the relationship between nitrogen flow and film depostion rate. The line was added as an estimate and each point is a single measurement.

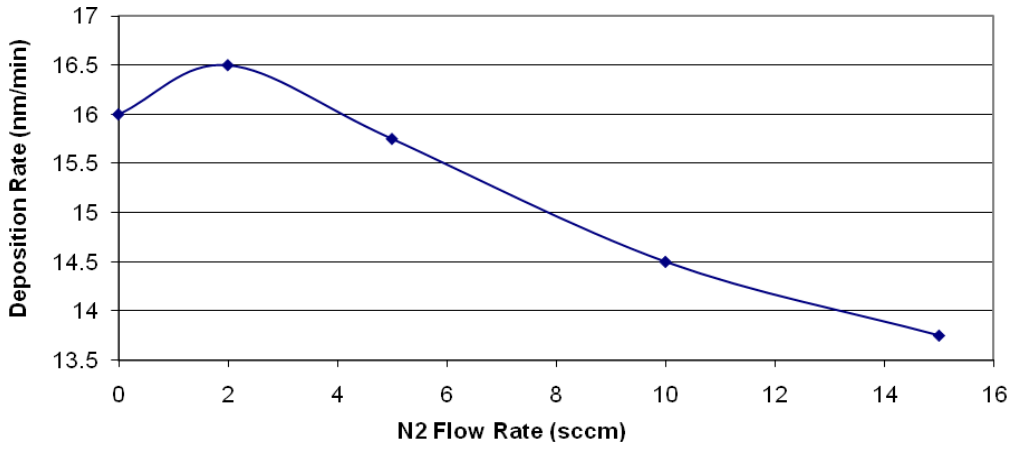

Figure 4.4 The effect of nitrogen flow rate on tantalum nitride deposition rate with a sputter pressure of 0.93 Pa and constant Ar flow rate of 50 sccm.

The deposition rate increased from 16.0 nm/min to 16.5 nm/min when nitrogen flow rate was increased from at 0 sccm to 2 sccm. It then decreased to 15.75 nm/min at 5 sccm,14.5 nm/min at 10sccm, and finally 13.75 nm/min at 15sccm.

The trend is consistent with the progressive formation of a charged resistive nitride layer on the surface of the target at high nitrogen partial pressures which repulsed incoming argon ions. At 0 to 2 sccm nitrogen, the target surface remained metallic due to sufficient discharge through bias reversal and ion flux. The constant ion flux reduced the thickness of the resistive nitride layer so the target surface remained metallic. While the sputtering rate of tantalum remained constant in this region, the additional incorporation of nitrogen increased the deposition rate. However, as the partial pressure of nitrogen increased the build up of nitrides on the target surface trapped positively charged ions. The resultant electric field reduced the incoming ion flux and reduced the deposition rate. Supporting evidence is seen in the hysteresis curve in Figure 4.5. Although the total amount of hysteresis from the curve is small, it still indicates the formation of an insulating layer as nitrogen flow increased.

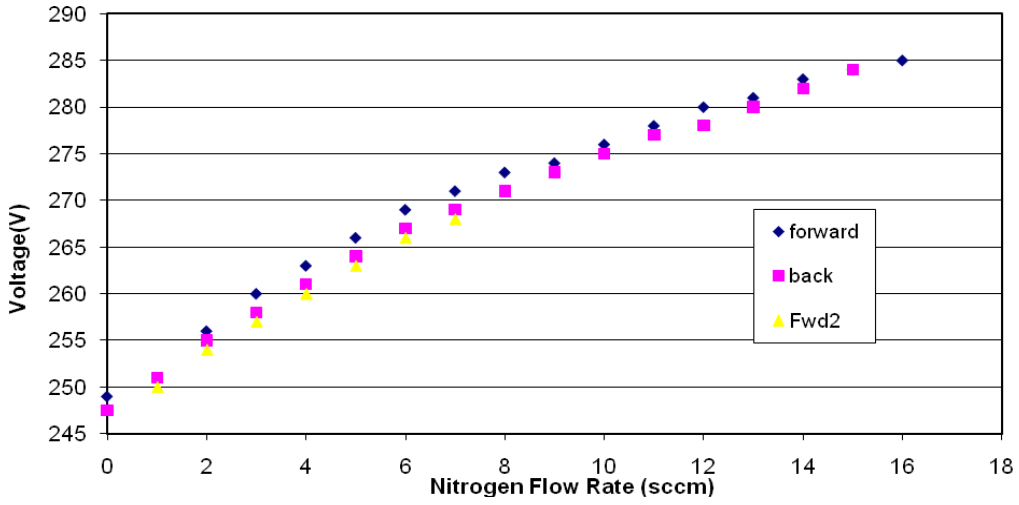

Figure 4.5 Hysteresis curve of Tantalum Nitride Sputtering Voltage

Compared to typical hysteresis, the tantalum nitride deposition showed a continuous increase in voltage without reaching a plateau region or abrupt transitions zone. This may be due to the fact that although the partial pressure of nitrogen was high within the chamber, the overall ratio of nitrogen to argon was still lower and there was not enough displacement by nitrogen to fully oxidize the surface of the target. However, there was a clear sign that the bias voltage was levelling toward an asymptotic value, after which only the highest nitride phase would remain.

From these observations, the metallic surface of the tantalum target began building a nitride layer at flow rates of 2 sccm and did not reach complete coverage at 20 sccm due to periodic discharge of electrons from the target surface via reverse biasing. Without charge build up, the flow of ions stayed constant along with the sputtering rate. The excess nitride layer was removed even at high partial pressures of nitrogen. However, the excess nitrogen and the adatoms were absorbed by the substrate surface, which increased the nitrogen to tantalum ratio of the film as the N_2 partial pressure increases. Due to the low substrate temperature, the exposed surface of the tantalum nitride film contained significant void spaces which oxidized and formed oxy-nitrides.

Three methods by which film quality could be improved were explored: either by increasing the substrate temperature, increasing the sputtering power, or reducing the sputtering pressure. Because of the operational constraints on the machine, sputtering pressure was the only optimization parameter available.

Experimentation showed film resistivity decreased and thickness variation increased as deposition pressure was reduced due to the increased beam directionality of the sputtered atoms. When sputtering pressure was increased the film resistivity increased and thickness variations decreased. Optimal nitrogen deposition pressure for stoichiometric tantalum nitride increased as the total deposition pressure was reduced. The optimized conditions for tantalum nitride deposition were total chamber pressure of 0.933 Pa, with flow rates of 50 sccm Ar, and 10 sccm of N_2 at which tantalum and nitrogen atomic percentage reached an asymptotic value as discussed in the next section.

4.6.Effect of nitrogen gas flow on composition of tantalum nitride

Surveys showed nitrogen and oxygen atomic percentage decreased with increasing length of ion etching; however they eventually reached minimum levels and rebounded as sample location neared the glass interface.

Film composition begins to level out at 10 sccm nitrogen flow as seen in Figure 4.6. The incorporation of oxygen is minimal at that flow rate. It can be assumed that a local optimal condition was reached at those parameters.

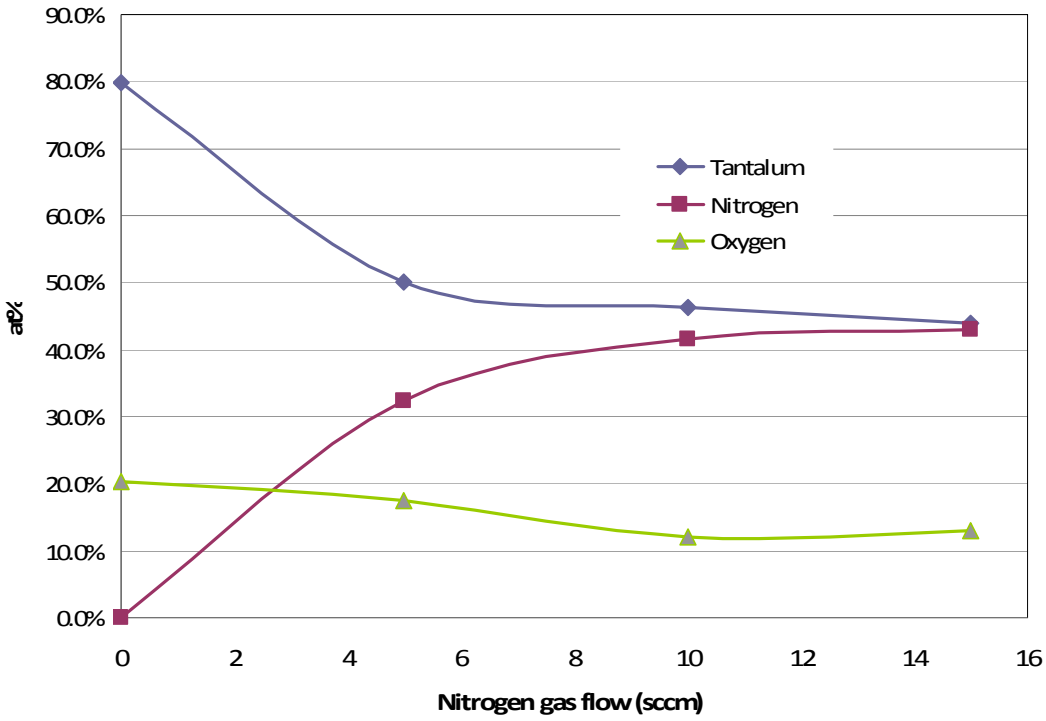

Figure 4.6 Composition of tantalum nitride with respect nitrogen pressure.

Figure 4.6 showed the nitrogen content is zero with no nitrogen flow, while oxygen began at 20.3 at% of the total. At 5 sccm, the nitrogen content ranged from 29.2% near the surface to 24.9% at the center of the film then to 25.0% near the glass interface. At above 2 sccm, the build up of a resistive nitride layer inhibited the dispersion of accumulated positive charge and reduced the deposition rate and this allowed more time for nitrogen to be absorbed onto the film as it grew. This was confirmed by XPS survey of TaN films deposited at 10sccm nitrogen. The nitrogen content of the film ranged from 38.2 at% near the surface to 32.8 at% inside the film, and back to 33.91 at% closer to the glass interface. At 15 sccm, the nitrogen content of the film varied from 39.4 at% near

the surface to 34.2 at% inside the film, and to 35.4 at% near the glass interface. The discrepancy between the internal and surface composition is due to the presence of tantalum nitride adsorbed atmospheric nitrogen compounds on the surface and the preferential sputtering of nitrogen to tantalum by the XPS ion gun. After 5 minute of ion sputtering before XPS surveys, the nitrogen to tantalum ratio dropped, while the atomic percentage of oxygen also decreased but eventually stabilized.

During analysis, XPS detected the presence of significant residual oxygen in tantalum films deposited under nitrogen and argon atmosphere, which was incorporated through absorbing oxygen and carbon from the deposition chamber or by atmospheric contamination in the columnar film. If the source was the deposition chamber, it was expected that the amount of oxygen would be constant as the XPS profile depth increased. However, the data indicated the oxygen content of the film is fairly constant throughout the thickness of the film. This supported the hypothesis that the carbon contaminations were from the atmosphere, while the oxygen content was incorporated during the deposition process.

The XPS survey of tantalum nitride films showed that the nitrogen to tantalum ratio of film increased from 0 to 0.649 as the nitrogen flow rate increased from 0 to 5 sccm. At higher flow rates of 10 sccm and 15 sccm, the nitrogen to tantalum ratio increased from 0.894 to 0.976, respectively. This showed that the rate of nitrogen incorporation consisted of two zones. In the first zone, from 0 to 10

sccm of N_2, the nitrogen to tantalum ratio increased rapidly with additional nitrogen partial pressure. In the second zone the rate of change with the addition of more nitrogen decreased and appeared to approach a fixed composition. The amount of oxygen in the films decreased as nitrogen flow rate increased from 0 to 10sccm. Total amount of oxygen decreased from 20.26 at% to a minimum of 12.13 at%. In conclusion, the optimal flow was 10 sccm of N_2 at 0.933 Pa working pressure.

4.7.Effect of Oxygen Flow Rate on Reactive Sputtering of TaO

In Figure 4.7, we see the hysteresis of the sputtering voltage when tantalum is sputtered in an argon oxygen plasma. The figure shows that the forward and the reverse voltages on target differed by a maximum of 3 V when using pulse power DC magnetron guns. This small difference may indicate the reverse bias was effectively neutralized during reverse bias cycles. However, it also indicated the surface layer of the target was not fully oxidized. When compared to the O/Ta ratio in Figure 4.8, this shows film composition reached stoichiometric tantalum oxide before the target surface was fully oxidized. The location of maximum oxygen to tantalum ratio and the early maximum in deposition rate implied that the majority of oxide formation was on the surface of the substrate. By maintaining oxygen flow rate at 10 sccm, the deposited film could achieve both stoichiometry and high deposition rate.

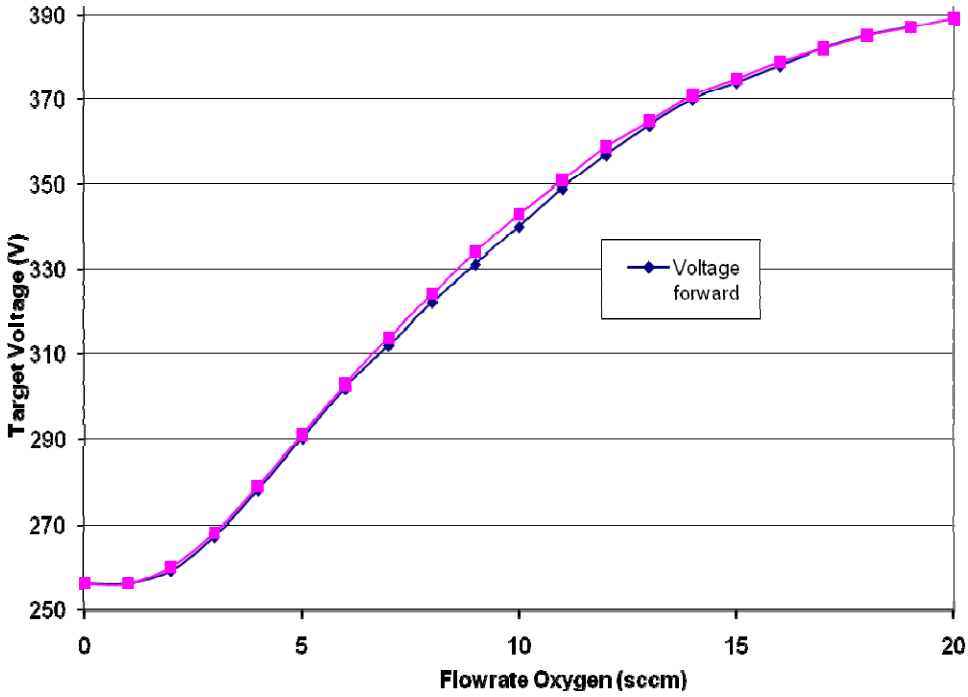

Figure 4.7 Target voltage hysteresis as a function of oxygen flow rate during the reactive sputtering of tantalum oxide with a sputter pressure of 0.93 Pa and constant Ar flow rate of 50 sccm. Each point was a single measurement

4.8.Composition of Ta_xO_y by XPS

Multiple surveys were made on tantalum and tantalum compound film samples. Surveys of tantalum films with no reactive gas flow were used to determine the effect of film morphology on composition. XPS done on these tantalum films showed 10 to 12 % oxygen composition at film depths of 15nm to 25nm. This indicated the films were either oxidized during deposition or post deposition due to porosity. If the oxygen was primarily due to porosity of the film, the amount of carbon contamination would reach a constant level with increasing film depth. Using an ion beam, the film was etched and sampled at various depths. The

composition averages are shown in Table 4.3, and graphically shown in Figure 4.8.

Table 4.3 XPS composition of tantalum pentoxide films deposited with a sputter pressure of 0.93 Pa and constant Ar flow rate of 50 sccm.

Sample ID	Reactant Gas	Gas Flow (sccm)	O at%	Ta at%	O/Ta
0	none	0	6.29	93.71	0.067
B	O_2	2	51.80	48.20	1.075
C	O_2	5	65.34	34.66	1.885
D	O_2	7.5	68.59	31.41	2.184
10	O_2	10	67.35	32.65	2.063
12	O_2	12	65.87	34.13	1.930
15	O_2	15	65.13	34.87	1.868

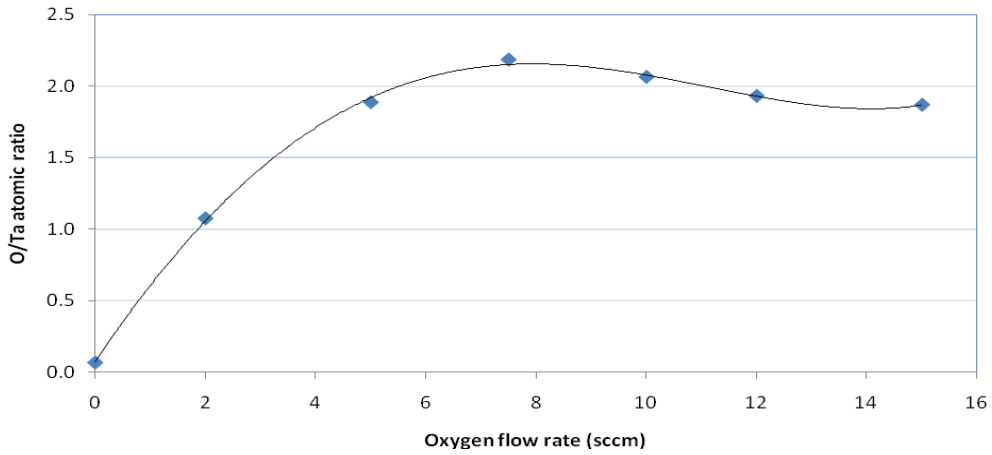

Figure 4.8 O/Ta atomic ratio as a function of oxygen flow rate with a sputter pressure of 0.93 Pa and constant Ar flow rate of 50 sccm. Each point was a single measurement

The atomic ratio of oxygen to tantalum increased from 0.12 at 0 sccm, peaked at 2.18 at 7.5 sccm oxygen flow, and then slowly declined at higher oxygen flow rates. By varying oxygen flow rate from 0 sccm to 15 sccm, while keeping constant chamber pressure during pulse power DC magnetron reactive sputtering, the oxygen to tantalum ratio varied from to 6.26 at% to 68.5 at%. From the shift of the oxygen 1s peaks of the XPS spectrum with respect to pure elemental oxygen, oxide formation began after the O_2 flow rate exceeded 2sccm.

4.9.The effect of oxygen partial pressure on the deposition rate of tantalum oxide

The deposition rate of tantalum oxide with respect to oxygen flow rate reached a maximum at 7.5 sccm oxygen flow, see Figure 4.9 below. This suggested that tantalum pentoxide formed primarily by tantalum oxidation on the substrate surface.

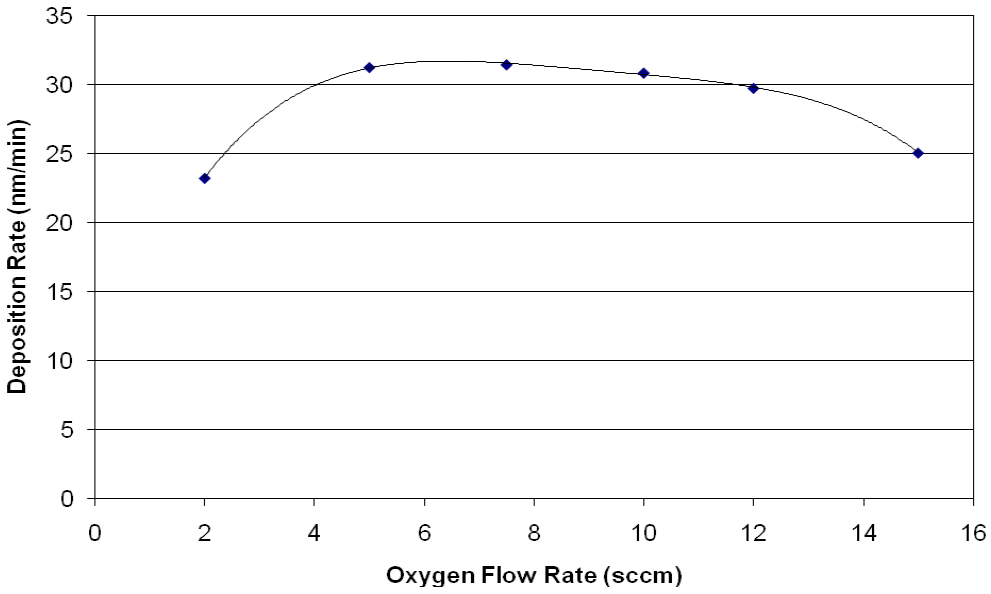

Figure 4.9 Deposition Rate of Tantalum Oxide as a function of oxygen flow rate with a sputter pressure of 0.93 Pa and constant Ar flow rate of 50 sccm.

The relationship between deposition rates and oxygen flow rate appeared to fit a 4^{th} order polynomial curve. From the graph in Figure 4.7, there was a difference of a single volt between the voltage when the oxygen flow rate was increased and when it was decreased. This indicated that the surface of the target was predominately metallic during the deposition process, and the reverse bias was large enough to remove the accumulated charge. It was noted that the maximum deposition rate also coincided with the maximum O/Ta ratio; as shown in Figure 4.8.

4.10. Optical characteristics of Tantalum Oxide on Glass by Variable Angle Spectroscopic Ellipsometry

During deposition, a high oxygen partial pressure was maintained to ensure that large proportion of the oxide film was composed mainly of stoichiometric tantalum pentoxide. Spectroscopic scans were performed using variable angle spectroscopic ellipsometry or VASE to measure the index of refraction using the change in polarization across the spectrum range of 300 to 1700nm. The values were then compared to bulk values.

Optical measurement of Reflectance and Transmission spectroscopic ellipsometry on the tantalum pentoxide layer showed that its refractive index ranged from 2.55 to 2.10 at wavelengths of 300nm to 1700nm. Comparisons with the results of He[45] indicate an amorphous film with oxygen deficiency possessed a higher index of refraction and low absorption coefficient as compared to theoretical crystalline stoichiometric tantalum pentoxide films.

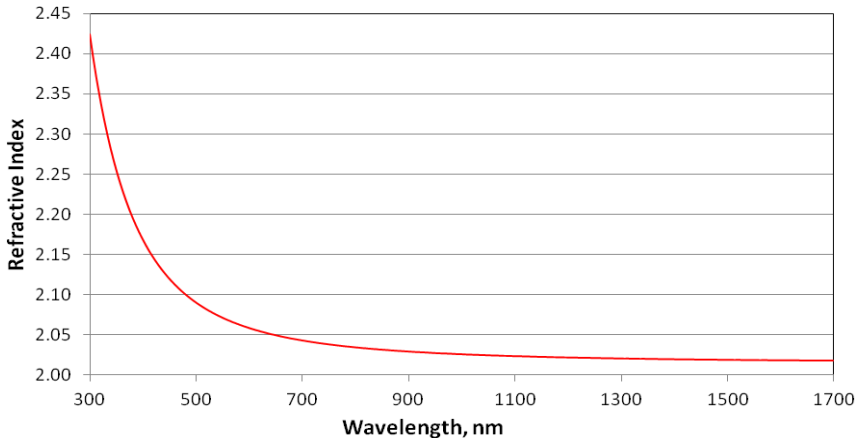

Figure 4.10 The refractive index of tantalum pentoxide grown for this study at oxygen flow rates of 10 sccm and greater.

The value of optical constant n(633nm) = 2.05 at 10sccm is close to the results of Ngaruiya [46], n(633nm)= 2.09 at 15 sccm O_2, and Chen [15], n(633nm)=2.08 at 30 sccm O_2 where it was shown that pre annealed samples from magnetron sputtering are typically amorphous films with higher index of refraction than recrystallization crystalline films.

Figures 4.11, 4.12 and 4.13 show light transmission through films deposited at 5, 7.5 and 10 sccm O_2 respectively.

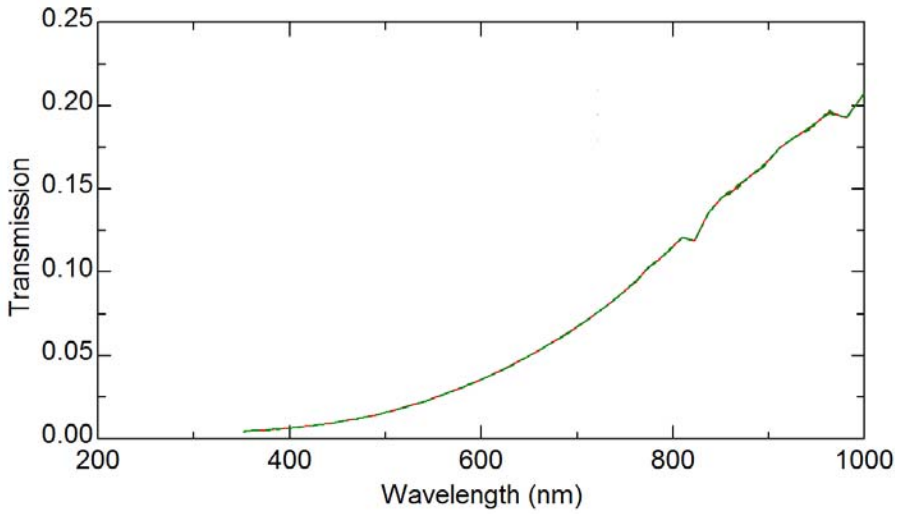

Figure 4.11 Optical transmission dispersion curve for Ta-O film deposited at 5 sccm oxygen flow rate.

Transmission through the tantalum oxide films indicated that at oxygen flow rates of 5 to 7.5 sccm the optical response of sputtered film transforms from metallic thin film to dielectric.

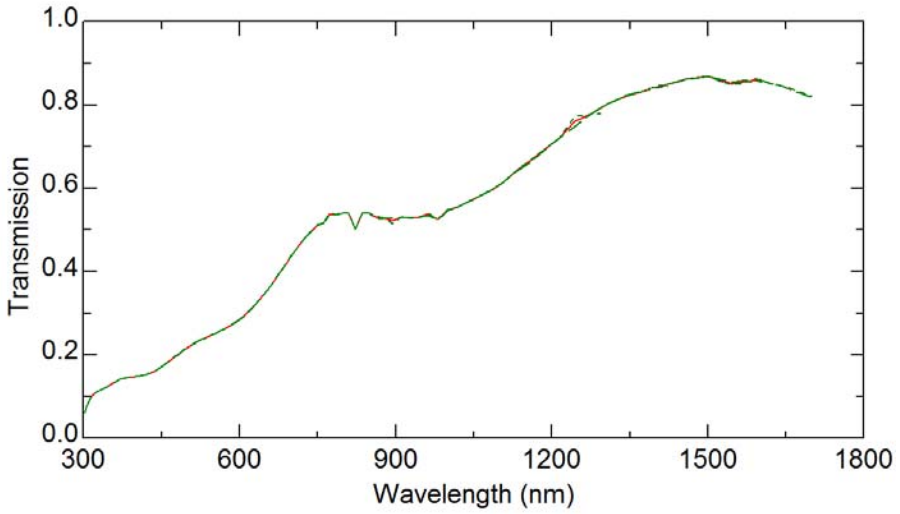

Figure 4.12 Optical transmission dispersion curve for Ta-O film deposited at 7.5 sccm oxygen flow rate.

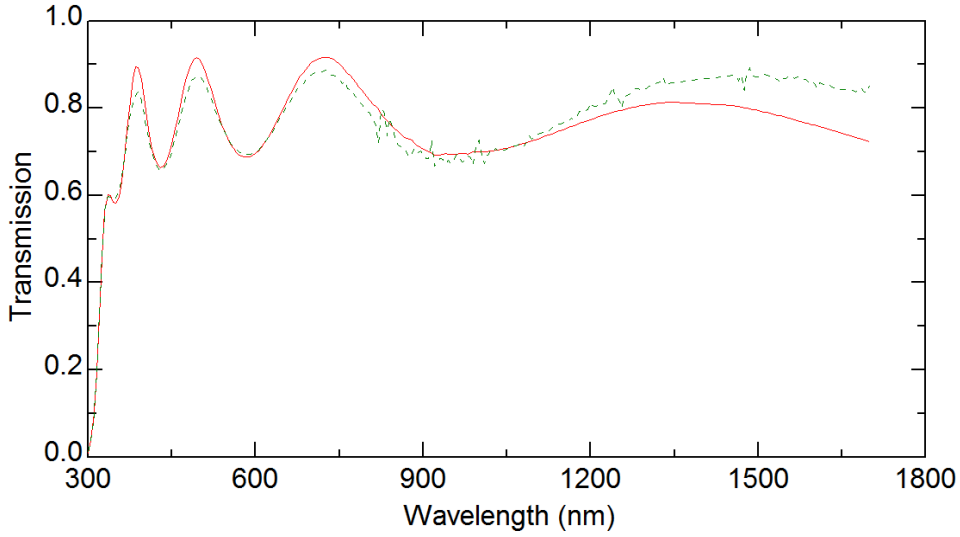

Figure 4.13 Optical transmission dispersion curve for Ta-O film deposited at 10 sccm oxygen flow rate.

At oxygen flow rates of 10 sccm and above, the index of refraction at 632.8nm was 2.05. Contrary to XPS results, which indicated the composition of the oxide films plateau at around 68.5 at% oxygen when O_2 flow was at 7.5sccm, the

transmission scans showed that tantalum pentoxide required a minimum 10sccm of O_2 flow rate to achieve desired optical and electrical insulation properties. Referring to Figure 4.12 and 4.13, the interference fringes in Ta-O film fully formed at 10 sccm oxygen flowrate while at 7.5 sccm the film is still strongly absorbent. Further support is the appearance of strong absorption at ~310nm in figure 4.13, which coincide with the amorphous tantalum pentoxide bandgap energy of 4.0eV as stated in literature.

4.11. Fabrication of Test Structures

4.11.1. Design of TaN resistor

To prevent oxide break down due to localized concentration of electric charges the serpentine resistors were designed to curve at each bend instead of having the typical squared corners. To fabricate the device, masks for resistors, contacts, and access vias were drawn on L-edit into five separate layers as shown in Figure 4.14.

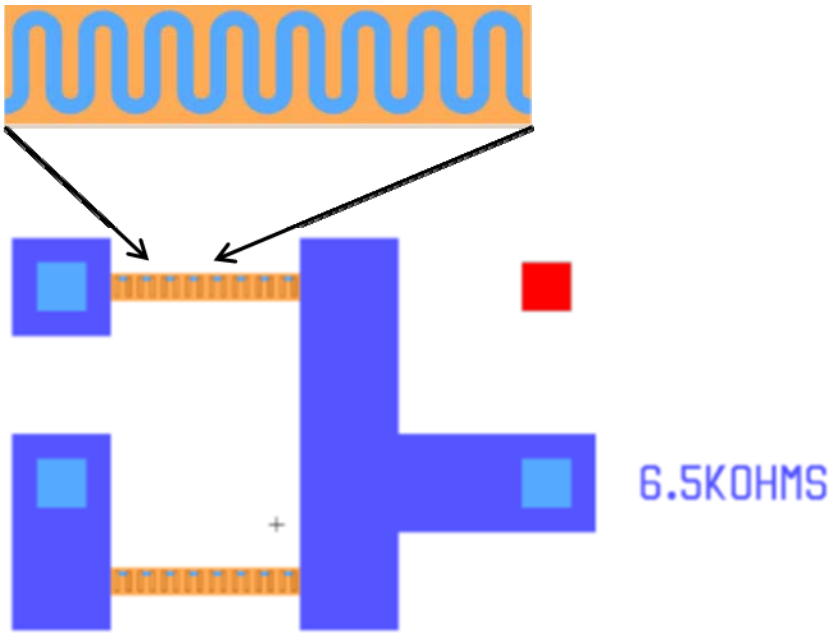

Figure 4.14 Design of the pH showing a blow-up image of the resistor

Each device contained a pair of serpentine resistors with the same dimensions. The top resistor was used as reference to indicate performance and to compensate for temperature effects. The pattern of the lower resistor was distanced from the two bottom pads to isolate the liquid contact from the electrical contacts.

4.11.2. Integration Process Flow

The proposed process flow for producing the pH measuring device is shown in Figure 4.15. Aluminum was initially used for the device backside contact. Due to low resistance in Ta_2O_5 films the contact metal was changed to chromium. The current process flow was the product of compromises between film quality and process compatibilities.

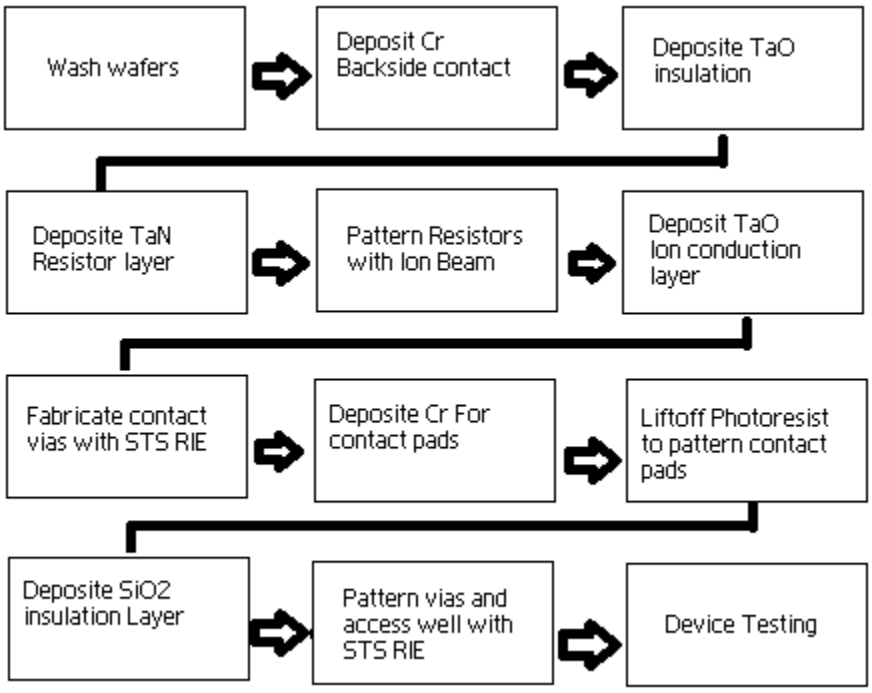

Figure 4.15 Process Flow for pH Sensor

During tantalum nitride deposition it was found that sheet resistance could vary by up to 10 percent between sessions with the same deposition parameters. The cause was the 6 to 10 percent variation in film thickness due to the chamber conditions and the Gaussian profile of sputtered atoms with a small target to substrate size ratio. Substrate rotation was used to reduce the influence of the uneven deposition. To achieve a more uniform film, a dedicated apparatus for tantalum nitride deposition with a larger target would be required. These are not available in the current operations. Annealing the tantalum nitride films after deposition should stabilize the resistivity, but equipment was not available.

Both wet and dry etching methods were used on the tantalum pentoxide and tantalum nitride layers. However, due to the high corrosion resistance of tantalum

compounds, the only etchant available was, hydrofluoric acid, which does not have high oxide/nitride selectivity, and the difficulty in controlling the etch rate, dry etching methods were used to control both the etch depth and profile.

4.11.3. Issues and Challenges

The probe height h had a significant effect on the observed resistance value through the ion conductor due to the relatively poor conductivity of the pH solution compared to the oxide. Currently, the resistance of the solution is in series with the measurement. In addition, an electric field emanates from the tip of the probe. This issue could be resolved by testing the device with the tips touching the oxide; the final device functionality may be impacted. Tentative testing indicates that there is minimal change to the current setup.

A coating of Ag/AgCl on the bottom of the recess instead of on the probe tip might be considered. This may significantly improve the current through the device.

There is some concern that by locating the recess over the serpentine, some of the current may be blocked. There is research that indicates nitrogen can alter the ion current in the oxide. There was also across wafer non uniformity, which would likely cause die to die variation in pH responses. It is proposed that the device design be changed by relocating the test well away from resistor.

4.12. Test Structure Results

4.12.1. pH responses from preliminary test on prototypes

Testing of pH devices showed that the current design would respond to changing pH; however, the reliability with respect to repeated measurements and sensitivity at high pH was poor and would require additional optimization. Looking at Figure 4.16 below there was a potential exponential response between the resistances of the ion conductor and the pH of the solution. It was found that the magnitude of the standard deviation of the data to be similar to the magnitude of the difference of the pH responses. This challenge was resolved by reviewing the data and removing the outlying measurements. By removing them the standard deviation dropped by half, but the pH response remained the same. This indicated that the device was working properly.

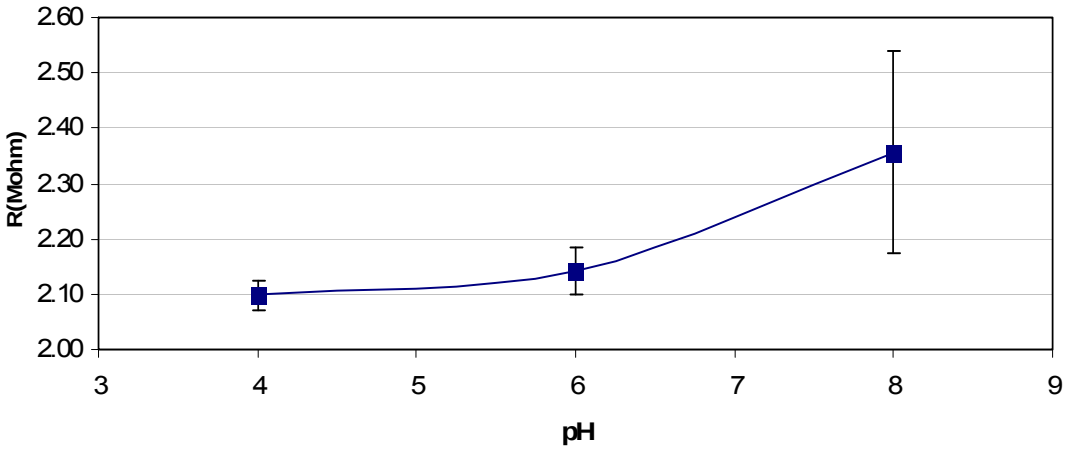

Figure 4.16 Resistance between contacts B-D on the pH device versus pH.

The upward curve of the pH response was expected from the channel model as the number of interstitial ions dropped logarithmically with increasing pH, the resistivity would increase exponentially as the number of activated channels decreased. The large standard deviation, was due to difference between devices and discrepancies in measurements. The resistance measurement was done by supplying a constant current through the oxide and then measuring the voltage difference between the backside contact and the oxide probe. The cathode was on top of the oxide and anode on the backside contact. When the polarity was reversed the resistance of the oxide did not vary proportionally with pH. In Figure 4.17 retested devices yielded a very different pH response, but the general trend of decline in resistance with exposure to increased pH levels was maintained for all devices.

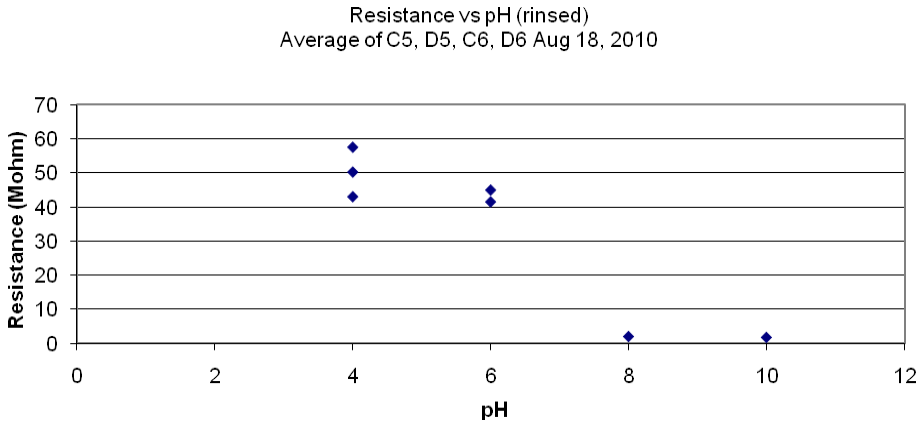

Figure 4.17 Aug 18, 2010 pH response of devices on wafer 5, the resistance value of the paired resistors ranges from 62MΩ to 1.59MΩ from pH value of 4 to pH value of 10 respectively.

During retesting the backside electrode oxidized and tantalum pentoxide delaminated as the pH testing progresses, until finally the device short circuited. The oxidation occurred in set locations that were typically directly beneath the probe tip. The discoloration of the oxidation spread from their initial points with applied current. These issues are not critical to our project since the final device is only expected to be used once.

4.13. Resistance Values and Device Yield across the wafer

One silicon wafer patterned is shown in Figure 4.18. Using wafer number 5, we calculated the typical yield as 9/14. The 5 failures are due to short circuiting between resistor contacts and the backside contact.

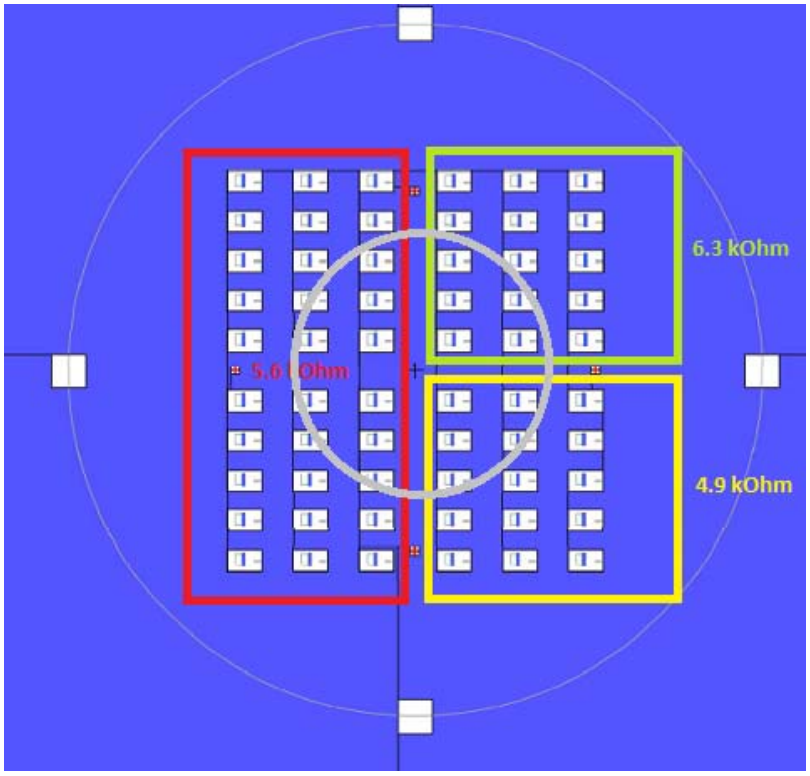

Figure 4.18 Wafer Layout

In Figure 4.19, device location is denoted by numbers and letters. Numbers denotes the device vertical location with respect to the upper left hand corner with lower number closer to the reference point. The letters denotes the devices horizontal location with respect to the upper left hand corner with A closest to the reference point. R_u is the resistance value of the upper resistor, R_l is the resistance value of the lower resistor, and B_s is the resistance value between the backside contact 2 and contact 4. Resistances are in kΩ.

Nov9/09	Resistor	kΩ					
		A	B	C	D	E	F
2	R_u	5.6815					5.4561
	R_l	5.7423					5.4126
	B_s	OV					OV
3	R_u		4.3591			4.7128	
	R_l		4.2371			4.617	
	B_s		100			129.4	
4	R_u			4.099	4.5414		
	R_l			4.094	4.4941		
	B_s			OV	OV		
5	R_u						
	R_l						
	B_s						
6	R_u			4.1632	4.1131		
	R_l			4.1904	4.0724		
	B_s			OV	OV		
7	R_u			4.2085	3.5893		
	R_l			4.1748	3.5875		
	B_s			412	OV		
8	R_u		NA			NA	
	R_l		NA			NA	
	B_s		7.8703			12.3	
9	R_u	4.4742					4.1131
	R_l	4.7329					4.0724
	B_s	OV					OV

Figure 4.19 Resistor values and device yields across a typical wafer (#5)

Green square denotes working devices, red squares are short-circuited devices, and yellow squares are devices that were not tested. When the B_s value is OV, the resistors and the backside contacts are in open circuit, and thus the devices would function as designed. If the value was lower than 100 kΩ then the oxide layer was short circuited by filaments of tantalum nitride, and rendered the device non-

functional. Increases in the magnitude and difference between resistor values R_u and R_l are seen in the above Table, indicated systematic thickness variation in the tantalum nitride layer. Typical thicknesses of the films deposited in orders are: 135nm of Cr, 145nm of Ta_2O_5, 125nm of TaN, 150nm of Ta_2O_5, ~800μm of SiO_2, and 135 nm of Cr.

The position of short-circuits between the outer rings and inner four devices, indicated there was a local minimum in oxide thickness due to bias in either deposition or ion milling. Review of our integration process showed that the effects of sputtering non-uniformity and etch bias of the ion beam are cumulative. The position of maximum deposition also coincided with the minimum ion sputtering at the center of the wafer.

4.14. Future Experiments

Before a demonstrable pH measuring device can be made there is much remaining work.

- Optimize the resistors. Modeling by our partner has shown that the optimum resistance should be 10 kΩ. We need to optimize and stabilize the TaN resistivity. An inert gas furnace could be use to anneal the TaN to stabilize its resistivity.

- Optimize the ion conduction of Ta_2O_5. This may obtain higher currents through varying oxide thickness, stoichiometry, etc. A quick turn test would speed up development; a fixed testing rig is now being considered.

- Relocate the ion sensing window to locations away from tantalum nitride layer to improve uniformity.
- Increase the distance between the contact pads. This would prevent the liquid from touching the pads
- Deposit a porous Ag/AgCl coating on top of the ion conducting window to create a uniform current flow through the oxide.
- Increase number of test devices wafers for evaluation, such as several good wafers with 10 kΩ resistors.

Plans for the far future include:

I. Investigate packaging options with ACAMP.

II. Investigate testing optimized devices with blood samples.

Chapter 5: Conclusion

Using DC magnetron reactive sputtering, tantalum nitride and tantalum oxide films were produced. Their composition and optical properties were assessed as a function of reactive gas flow rates. Results indicated that nitrogen gas flow both controlled the resistivity of sputtered tantalum nitride and suppressed the incorporation of oxygen. VASE transmission on tantalum oxide with various oxygen pressure indicated insulating oxide forms only when the target enters oxide mode at 10^{+} sccm of oxygen flow. The VASE result and XPS surveys on tantalum oxide films showed that stoichiometric tantalum pentoxide was deposited. The bandgap of the transparent tantalum oxide at 10 sccm oxygen was ~4.0 eV, which indicated the material as amorphous tantalum pentoxide. Across the wafer, resistor values were below their design value with lower resistance toward the center of the wafer. The difference in resistance between resistors ranged from below 1 percent near the center of the wafer to 5.78 percent at the edge. These indicated systematic non-uniformity in film thickness. There were indications of the tantalum pentoxide insulation layer having pores and other perforating defects by the number of short circuited devices situated between the inner and the outermost devices. Preliminary result on pH response of the various devices indicated the resistance of the device decreased with decreasing pH. This fits the hypothesis that increasing availability of free ions would increase the conduction through thin amorphous tantalum pentoxide as outlined by the channel model. Evidence of ion conduction through channels and open structures was also evident by the localized oxidation of the backside contact during subsequent

pH testing. While performing tests on the devices it was found that repeated exposure to different pH solutions changed the device behaviour. Fabrication yields of the devices were poor and may require further work to optimize or change film material to achieve design functions.

[1] Lee, S, Texture, structure and phase transformation in sputter beta tantalum coating, Surface and Coatings Technology, 44 (2004), 177-178

[2] Leszek Gladczuk, Tantalum films for protective coatings of steel, Thin Solid Films 467 (2004) 150– 157

[3] D. Gerstenberg, Properties of Tantalum Sputtered Films, Electronics Reliability Microminiaturization, Pergamon Press 1962. Vol. 1, pp. 353-358.

[4] I. Petrov, Microstructural evolution during film growth, J. Vac. Sci. Technol. A 21.5., Sept/Oct 2003, S117-S128

[5] T. Riekkinen, Reactive sputter deposition and properties of Ta N thin films, Microelectronic Engineering 64 (2002) 289–297

[6] H. Okamoto, N-Ta (Nitrogen-Tantalum), Journal of Phase Equilibria and Diffusion Vol. 29 No. 3 2008, pp 291

[7] Xin Sun, Properties of reactively sputter-deposited Ta-N thin films, Thin Solid Films, 236 (1993) 347-351

[8] C. Stampfl, Stable and metastable structures of the multiphase tantalum nitride system, Physical Review B 71, 024111 (2005)

[9] Aditya Aryasomayajula, Pulsed DC magnetron sputtered tantalum nitride hard coatings for tribological applications, Surface & Coatings Technology 201 (2006) 4401–4405

[10] S.M. Kang, Control of electrical resistivity of TaN thin films by reactive sputtering for embedded passive resistors, Thin Solid Films 516 (2008) 3568–3571

[11] C. Chaneliere, J.L. Autran, R.A.B. Devine, B. Balland, Tantalum pentoxide (Ta2O5) thin films for advanced dielectric applications, Materials Science and engineering, R22 (1998) 269-322 R Reports: A Review Journal

[12] Tajima, Effective Density of Tantalum Oxide Thin Film by Reactive DC Magnetron Sputtering for All-Solid-State Switchable Mirror, Journal of The Electrochemical Society, 154 9 J267-J271 2007

[13] S.P. Garg et al, The O-Ta (oxygen-tantalum) system, Journal of Phase Equilibria [1054-9714] yr:1996 vol:17 iss:1 pg:63-77

[14] Ke Wang, In Situ Spectroscopic Observation of Activation and Transformation of Tantalum Suboxides, J. Phys. Chem. A 2010, 114, 2489–2497

[15] K. Chen, Study of Amorphous Reactive Sputtering Ta_20_5 Thin Films by DC Magnetron, Journal of Electronic Materials, Vol. 26, No. 4, 1997, pg:397-401

[16] Cevro and Carter, Ion-beam and dual-ion-beam sputter deposition of tantalum oxide films, Optical Engineering [0091-3286] yr:1995 vol:34 iss:2 pg:596-606

[17] D M Hughes, Electrical conduction in reactively sputtered tantalum oxide thin films, J. Phys. D: Appl. Phys., Vol. 7, 1974

[18] Sheng-Ren Chang, A CMOS-Compatible, Low-Noise ISFET Based on High Efficiency Ion-Modulated Lateral-Bipolar Conduction, Sensors 2009, 9, 8336-8348

[19] S.P.L. Sörenson, Biochemische Zeitschrift, 21, 1909, pp.131-200

[20] http://goldbook.iupac.org/P04524.html 2011-02-08

[21] P. M. Harve, Beckman pH Meters, http://www.sasta.co.za/wp-content/uploads/Proceedings/1950s/1955_Harvey_Beckman%20Ph%20Meters.pdf 2011-02-08

[22] Yuri G. Vlasov, Analytical applications of pH-ISFETs, Sensors and Actuators 8, I0 (1992) I-6

[23] Tubandt , Zeitschrift fur Elektrochemie und Angewandte Physikalische Chemie, Volume: 39 Pages: 227-244 Published: 1933

[24] C.P. Bean, J. C. Fisher, and D. A. Vermilyea, Ionic Conductivity of Tantalum Oxide at Very High Fields, Physical Review, Vol 101, no 2, (1956)

[25] L. Young, Theory of Ionic Conduction in Solids, Canadian Journal of Chemistry. VOL. 50, 1972

[26] K. Lehovec, Space-charge layer and distribution of lattice defects at the surface of ionic crystals, The Journal of Chemical Physics [0021-9606] yr:1953 vol:21 iss:7 pg:1123-1128

[27] Duggan, Ionic-Conductivity Of Tantalum Oxide By RF-Sputtering, Solid State Ionics [0167-2738] yr:1993 vol:62 iss:1-2 pg:15-20

[28] Tadahiko Saito, Properties of Tantalum Oxide Thin Film for Solid Electrolyte, Solid State Ionics 40/41 (1990) 499-501

[29] J.C. Chou, Comparison of the pH sensitivity of different surfaces on tantalum pentoxide, Sensors and Actuators B 65 2000. 237–238

[30] Can Xu, Masters Thesis, University of Alberta, 2010

[31] J.A. Thornton, Annual Review Material Sciences, 7, 239, 1977

[32] Fleming, Defect dominated charge transport in amorphous Ta2O5 thin films, Journal of Applied Physics [0021-8979] yr:2000 vol:88 iss:2 pg:850-862

[33] William D. Callister, Jr. Materials Science and Engineering An Introduction, 6th, 2003. , pp 761

[34] A.K. Kulkarni, Electrical and structural characteristics of chromium thin films deposited on glass and alumina substrates, Thin Solid Films [0040-6090] yr:1997 vol:301 iss:1-2 pg:17-22

[35] Kazuki Tajima, Solid electrolyte of tantalum oxide thin film deposited by reactive DC and RF magnetron sputtering for all-solid-state switchable mirror glass, Solar Energy Materials & Solar Cells 92 (2008) 120–125

[36] S. Capone, Physical characterization of hafnium oxide thin films and their application as gas sensing devices, J. Vac. Sci. Technol. A 16.6., Nov/Dec 1998

[37] Peter Broqvist, Amorphous hafnium silicates: structural, electronic and dielectric properties, Microelectronic Engineering 84 (2007) 2416–2419

[38] S. Banerjee, Physics and chemistry of photocatalytic titanium dioxide: Visualization of bactericidal activity using atomic force microscopy, Current Science, VOL. 90, NO. 10, 25 May 2006

[39] E. Krogh Andersen, Proton Conduction In $H_2Ti_40_9$, 1.2 H_20, Solid State Ionics 27 (1988) 181-187

[40] Atsushi Kawamoto, Journal of Applied Physics, 1 Augest 2001, VOL 90, No 3

[41] S. Vizzini, Controlled growth of aluminum oxide thin films on hydrogen terminated Si(0 0 1) surface, Journal of Crystal Growth 305 (2007) 26–29

[42] F. Paumier, Yttrium oxide thin films: chemistry stoichiometry-strain and microstructure, Crystal Engineering 5 (2002) 169–175

[43] Man Feng, Ionic conduction of $Ba_3Y_40_9$, Solid State Ionics 68 (1994) 269-277

[44] F Messina, Generation of defects in amorphous SiO2 assisted by two-step absorption on impurity sites, J. Phys.: Condense Matter 20 (2008) 275210 (6pp)

[45] Xiliang He, Characterization of high quality tantalum pentoxide film synthesized by oxygen plasma enhanced pulsed laser deposition, Thin Solid Films 518 (2009) 94–98

[46] J. M. Ngaruiya et al, Preparation and characterization of tantalum oxide films produced by reactive DC magnetron sputtering, Phys. Stat. Sol. (a) 198, No. 1, 99– 110 (2003)